

AD-A190 909

COMPUTER TOMOGRAPHY AND HYBRID OPTICAL/DIGITAL METHODS
FOR AERODYNAMIC ME. (U) MICHIGAN UNIV ANN ARBOR DEPT OF
MECHANICAL ENGINEERING AND AP. C H VEST 28 DEC 87

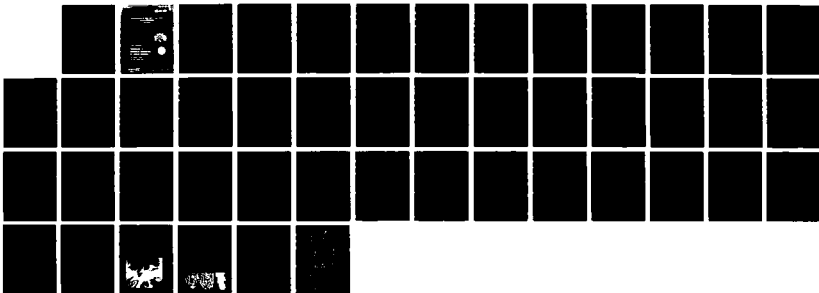
1/1

UNCLASSIFIED

ARO-20740. 5-EG DAAG29-83-K-0139

F/O 1/1

NL



1·0

2·8

2·1

3·15

2·0

1·1

3·5

2·0

4·0

4·5

1·8

1·25

1·4

1·6

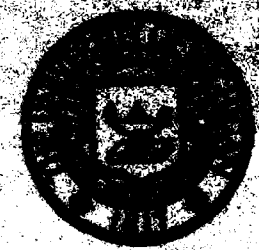
AD-A190 909

College of Engineering

Department of
Mechanical Engineering
& Applied Mechanics

The University of Michigan
Ann Arbor, Michigan 48109

STAMP



EXPERIMENTAL MECHANICS
Approved for public release
Distribution Unlimited

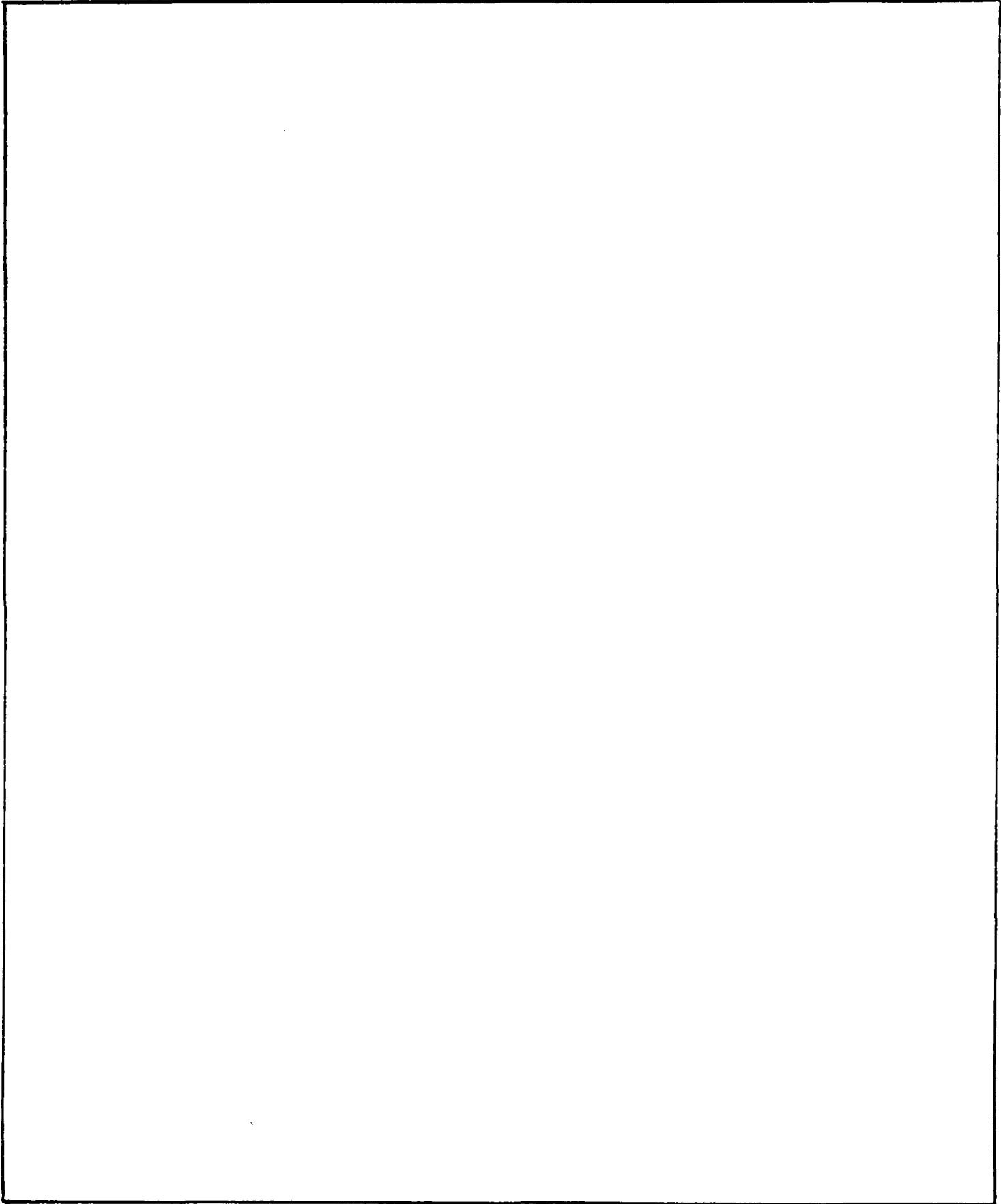
88 1 27 070

REPORT DOCUMENTATION PAGE

1a. REPORT SECURITY CLASSIFICATION Unclassified		1b. RESTRICTIVE MARKINGS	
2a. SECURITY CLASSIFICATION AUTHORITY		3. DISTRIBUTION/AVAILABILITY OF REPORT Approved for public release; distribution unlimited.	
2b. DECLASSIFICATION/DOWNGRADING SCHEDULE		4. PERFORMING ORGANIZATION REPORT NUMBER(S)	
4. PERFORMING ORGANIZATION REPORT NUMBER(S)		5. MONITORING ORGANIZATION REPORT NUMBER(S) ARU 20740.5-EC	
6a. NAME OF PERFORMING ORGANIZATION The University of Michigan	6b. OFFICE SYMBOL (if applicable)	7a. NAME OF MONITORING ORGANIZATION U. S. Army Research Office	
6c. ADDRESS (City, State, and ZIP Code) Dept. of Mechanical Engineering Ann Arbor, MI 48109		7b. ADDRESS (City, State, and ZIP Code) P. O. Box 12211 Research Triangle Park, NC 27709-2211	
8a. NAME OF FUNDING/SPONSORING ORGANIZATION U. S. Army Research Office	8b. OFFICE SYMBOL (if applicable)	9. PROCUREMENT INSTRUMENT IDENTIFICATION NUMBER DAAG29-83-K-0139	
8c. ADDRESS (City, State, and ZIP Code) P. O. Box 12211 Research Triangle Park, NC 27709-2211		10. SOURCE OF FUNDING NUMBERS	
		PROGRAM ELEMENT NO.	PROJECT NO.
		TASK NO.	WORK UNIT ACCESSION NO.
11. TITLE (Include Security Classification) Computer Tomography and Hybrid Optical/Digital Methods for Aerodynamic Measurements			
12. PERSONAL AUTHOR(S) C.M. Vest			
13a. TYPE OF REPORT FINAL	13b. TIME COVERED FROM 1-1-84 TO 31-8-87	14. DATE OF REPORT (Year, Month, Day) 1987, December 28	15. PAGE COUNT 40
16. SUPPLEMENTARY NOTATION The view, opinions and/or findings contained in this report are those of the author(s) and should not be construed as an official Department of the Army position, policy, or decision, unless so designated by other documentation.			
17. COSATI CODES		18. SUBJECT TERMS (Continue on reverse if necessary and identify by block number)	
FIELD	GROUP	Tomography, computer tomography, holography, interferometry, holographic interferometry, aerodynamics, refraction, jets, turbulent jets	
19. ABSTRACT (Continue on reverse if necessary and identify by block number) A hybrid optical/digital system has been developed to measure instantaneous, three-dimensional, density distributions in aerodynamic flows. The system uses a pulsed laser and discrete phase-step holographic interferometry, resulting in excellent phase resolution and a substantial level of automation of phase readout. The system uses reflection-, as well as transmission-, holography. Data are analyzed by computer tomography using a new algorithm (constrained iterative convolution) developed during this program. The entire system was used to study turbulent helium jets, disclosing their basic structures. Research also was conducted to develop methods for computer tomographic analysis when the optical probing rays are bent due to strong refraction, e.g. around shocks. Two iterative methods and a perturbation analysis were developed and studied. For most applications the simple perturbation approach is recommended.			
20. DISTRIBUTION/AVAILABILITY OF ABSTRACT <input type="checkbox"/> UNCLASSIFIED/UNLIMITED <input type="checkbox"/> SAME AS RPT. <input type="checkbox"/> DTIC USERS		21. ABSTRACT SECURITY CLASSIFICATION Unclassified	
22a. NAME OF RESPONSIBLE INDIVIDUAL		22b. TELEPHONE (Include Area Code)	22c. OFFICE SYMBOL

UNCLASSIFIED

SECURITY CLASSIFICATION OF THIS PAGE



UNCLASSIFIED

SECURITY CLASSIFICATION OF THIS PAGE

I N T F L - 8 7 0 1

COMPUTER TOMOGRAPHY AND HYBRID OPTICAL/DIGITAL METHODS
FOR
AERODYNAMIC MEASUREMENTS

FINAL REPORT

C. M. Vest

U.S. Army Research Office

DAAG29-83-K-0139

The University of Michigan

Approved for Public Release;
Distribution Unlimited

Accession For	
NTIS GRA&I	<input checked="" type="checkbox"/>
DTIC TAB	<input type="checkbox"/>
Unannounced	<input type="checkbox"/>
Justification	
By	
Distribution/	
Availability Codes	
Dist	Avail and/or Special
A-1	

The view, opinions, and/or findings contained in this report are those of the author and should not be construed as an official Department of the Army position, policy, or decision, unless so designated by other documentation.

TABLE OF CONTENTS

1. INTRODUCTION.....1

2. PROBLEM STATEMENT.....1

3. SUMMARY OF IMPORTANT RESULTS.....3

 3.1 Digital Holographic Interferometry.....3

 3.1.1 System Description.....3

 3.1.2 Flow Visualization.....6

 3.2 Tomographic Code: Consistent Iterative Convolution..7

 3.3 Measurement of Turbulent Helium Jets.....8

 3.4 Tomography of Strongly Refracting Flows.....9

4. PUBLICATIONS.....12

 4.1 Journal Articles.....12

 4.2 Doctoral Dissertations.....12

 4.3 Presentations at Technical Meetings.....12

 4.4 Reports.....13

5. PARTICIPATING SCIENTIFIC PERSONNEL.....14

6. APPENDIX.....15

1. INTRODUCTION

This is the final report for the project entitled "Computer Tomography and Hybrid Optical/Digital Methods for Aerodynamic Measurements" sponsored in the Department of Mechanical Engineering and Applied Mechanics at The University of Michigan by the Army Research Office during the period 1 January 1984 through 31 August 1987.

2. PROBLEM STATEMENT

During this program of research we have explored several topics dealing with the use of hybrid optical/digital methods for recording, visualizing and measuring complex flow fields. The ultimate intent of this research was to develop a system based on digital holographic interferometry and computer tomography to determine the distribution of density in the cross section of complex three-dimensional aerodynamic flows. We have been successful in this endeavor.

Our work had three basic components. The first was the development of a hybrid system to record interferometric data for subsequent tomographic analysis. This system used digital holographic interferometry (also known as quasi-heterodyne holographic interferometry or discrete phase-step holographic interferometry). The system had to be capable of recording the data with a pulsed laser, had to record data for a large number of different viewing directions simultaneously and had to be interpretable in a relatively automated manner.

The second component of our work dealt with development of reliable methods for tomographic reconstruction of flows which give rise to significant refraction, or ray bending, of the laser light used to probe the flow. Ordinary computer tomography is based on algorithms which assume that probing rays are straight lines. In flows containing shocks or other steep gradients this assumption is not valid because the consequent variation of refractive index causes the probing rays to bend. The resulting problem of tomographic reconstruction is both nonlinear and ill-determined. A thorough study of both the optical and computational aspects of this problem was conducted and the techniques developed were compared in detail with previously developed methods appropriately modified to apply to aerodynamic measurements.

The third component of our research was the establishment of an appropriate computer tomography code for the analysis of complex flow data. Although the literature of computer tomography is extensive, existing codes did not appear to be satisfactory for our purposes. Therefore we set out to develop a new technique for iterative reconstruction of such fields.

Physical experiments were planned and carried out using a turbulent free jet of helium as the test flow. Although not originally anticipated, digital holographic interferometry turned out to form the basis of a useful new flow visualization system. This avenue of research was also explored and reported.

3. SUMMARY OF IMPORTANT RESULTS

In this section we outline the key results obtained during the research program. In most cases the results have been fully documented in journal articles, which are referenced in the text of this report.

3.1 Digital Holographic Interferometry

3.1.1 System Description

Digital interferometry is a recently developed hybrid optical-digital metrology technique combining two-exposure holographic interferometry with digital image acquisition and computer processing to determine the interferometric phase directly from a set of image irradiance measurements. The technique is similar to heterodyne holographic interferometry in that both manipulate the interferograms phase in a known manner to determine its magnitude. Because this technique requires only the recording of a sequence of irradiance values of each pixel in an image grid, it is particularly well suited to recording by vidicon or photodiode arrays and processing by digital computer. It bypasses many of the problems associated with analysis of interferometric fringe patterns and readily yields the sign as well as magnitude of phase shifts.

In this type of interferometry, a two exposure holographic interferogram is recorded. One exposure is made of the flow of interest and a second exposure is made with the fluid quiescent. Physically different reference waves are used for each of the two holographic recordings. At the time of reconstruction, the phase of one of these waves is changed by a known amount. Such

discrete phase changes are made at least three times and the consequent change of irradiance of each pixel of the image is recorded. Elementary mathematical manipulation enables one to calculate the unknown phase shift (optical pathlength change) caused by the flow at each image point. More than three measurements can be made thereby providing computational redundancy and suppressing some errors. The usual complicated fringe counting procedure is replaced by a simple, computational sorting operation.

In this research our ultimate objective was to make tomographic measurements of a turbulent jet; therefore, our system needed to instantaneously record interferograms corresponding to several different viewing directions. Our system was based on the use of a pulsed ruby laser. In the course of the experimentation it became clear that this laser needed to be modified in order to perform satisfactorily. A temperature-stabilized intracavity etalon was installed and thereafter the laser produced sufficient coherence and mode structure to perform the experiments.

The test section was a rectangular area through the center of which a free helium jet flowed. In order to maximize the number of viewing angles available, two sides of this rectangular test section were glassed difusers illuminated from behind by the pulsed laser. The other two walls of the rectangle held glass photographic plates on which the holograms were recorded. In order to get these holograms as close as possible to the jet thereby maximizing the solid angle of view available one of these holograms was a traditional transmission hologram while the other

was a reflection hologram. A reflection hologram is one in which the reference wave and object wave enter opposite sides of the holographic plate and the holographically reconstructed object wave is formed by reflection from the developed plate rather than by transmission. The development of this system required a significant amount of experimentation with reflection holograms. A variety of chemical processing techniques for development and bleaching of reflection holograms was tried and comparatively evaluated.

A reconstruction system using a helium-neon laser was constructed on a separate optical table. This system included a mirror mounted on a piezo-electric crystal with a feedback control system for varying the phase by known amounts and holding that phase stable during the reconstruction process. Irradiance data were recorded using a high quality Cohu video camera. Digitized images recorded in this manner were stored in a local LSI 11/23 microcomputer which was also used to analyze the phase shifts and to display computed images. Tomographic reconstructions were carried out either on The University of Michigan's mainframe IBM 3090 computer or on an Apollo computer workstation.

This basic system and technique is described in more detail in a paper entitled "Digital Interferometry for Flow Visualization" which is included in the appendix of this report and will be more fully described in a journal article currently in preparation.

3.1.2 Flow Visualization

An interesting and very useful sidelight of the research program was the development of a flow visualization technique based on digital holographic interferometry. Recall that the optical pathlength change, or phase shift, at each point in the image of the flow is a computed value. This is different than ordinary interferometry which directly results in an analog interference fringe pattern. It therefore is possible to display results in a number of ways. Ordinarily, one would display contours of constant phase shift, that is calculate an interferogram. However, if one displays a simple gray scale image, for example setting a value of zero to the largest phase shift occurring and a value of one to an undisturbed region of the flow, a remarkably clear visualization of the flow can be displayed. Such images are very similar in appearance to images formed by techniques such as laser induced fluorescence. The properties of such images are similar to traditional shadowgraphs except they are sharply in focus in the object plane of the camera used to record the image. Such images may be particularly useful for relatively weak flows, because the digital interferometric system is very accurate and can be used to record images that would result in less than a single fringe in an ordinary interferogram. This technique is recorded briefly in a paper in the appendix to this report as well as in the PhD thesis of David W. Watt, and will also appear in a journal article currently under preparation.

3.2 Tomographic Code: Consistent Iterative Convolution

In the current study we attempted to compute cross sectional images of a turbulent helium jet. This flow is relatively complex and requires a considerably greater amount of data than have been used for previous reconstructions in this laboratory. The question of how best to effect the tomographic reconstruction is not a simple one and was investigated in some detail during this research. We settled on the use of iterative convolution. This means that the fundamental reconstruction technique is the classical convolution algorithm. However, this algorithm assumes that experimental data are available for a full set of equally spaced viewing directions distributed over 180 degrees. This requirement could not be met in the experimental set up developed for this research, nor is it likely to be in most fluid dynamic experiments. Hence we developed an iterative technique in which the missing data are effectively replaced computationally. Such an iterative convolution technique was originally proposed by this laboratory under a previous ARO contract. However, the basic iterative convolution technique was not sufficiently accurate to handle the complexity occurring in this experiment, and its convergence properties were poor and poorly understood.

In order to analyze the data from this experiment we extended our previous work by developing a technique of constrained iteration between the estimated image of the flow and its Radon transform. (The Radon transform is the appropriate mathematical term for the set of line integrals of flow density obtained interferometrically.) We found that for certain test functions used to study this technique, the estimated image

diverges from the actual function. This divergence was shown to result from the algorithm's failure to enforce consistency between the image estimate and its measured Radon transform. Such consistency in the new approach is enforced using a routine based on the direct inversion formula and on decomposing the image into its measured and missing components. This routine was used to develop a new iterative algorithm which converges absolutely for all test functions studied.

The consistent iterative convolution technique and its behavior are described in detail in a journal article currently under preparation and also in the doctoral thesis of David W. Watt.

3.3 Measurement of Turbulent Helium Jets

The total system for holographic recording, digital image acquisition and processing, and tomographic reconstruction was developed and studied by examining free helium jets in air. The jets studied had Froude numbers varying from 160 to 37,500 and Reynolds numbers varying from 250 to 1250.

Prior to conducting tomographic reconstructions, we examined flow visualization images of several of the jets. These images tended to confirm contentions previously appearing in literature that such turbulent jets are organized into large scale motions whose length scale is of the order of the local flow width. The tomographic images of the cross sections of the jets clearly confirm the presence of nearly unmixed ambient fluid within the jet boundaries and indicated that these inclusions are responsible for steep concentration gradients within the jet.

These images also seem to show the presence of vortical motions in the off-center jet regions which result in medium scale (half the jet width or less) inclusions of ambient fluid. They also seem to confirm that the jet scalar field is divided into regions of largely constant concentration. It must be recognized that we did not conduct a detailed study of this turbulent flow and that the system we have constructed can "freeze" the entire three-dimensional flow field at an instant of time, but does not document the time dependent behavior of the jet. The images also are imperfect and contain certain experimental and reconstructional artifacts. Some of these difficulties stem from the fact that we used lasers of different frequencies for recording and reconstruction. Although we designed the setup to minimize apparent deformations caused by this wavelength shift, they are not eliminated entirely. Nonetheless, we consider these experiments to be highly successful and to show the practicality of making instantaneously three-dimensional measurements in complex flows.

3.4 Tomography of Strongly Refracting Flows

When strong density gradients occur within the flow field under examination, the probing optical rays may be significantly bent. In this case the well-known computer tomography algorithms, which assume probing rays to be straight lines, are not applicable. During this research program, we carried out an extensive study of tomographic reconstruction in the presence of such strong refraction. Related problems are somewhat better explored in the context of acoustical and ultrasonic problems.

Distinct differences arise when optical problems are considered. In this research we posed the problem in the optical context. The resulting mathematical problem is highly nonlinear, and we approached it by two iterative techniques and a perturbation analysis.

The first procedure is called straight line inversion with modified data (SLIM) and is based on previous work by Bates and McKinnon and by Cha and Vest. This is essentially a method of successive approximations in which an initial estimate of the field is computed by ignoring the refraction effects and then iteratively corrected by using computational ray tracing to effectively calculate an interferogram which can be compared with the measured data. The second iterative technique is referred to as the curved ray algebraic inversion (CRAI). This is based on earlier work of Johnson and of Schomberg. In this procedure the current estimate of the index of refraction is used to generate a system of algebraic equations where the unknowns are corrections to this estimate at each pixel. In a sense it is a modified version of the well-known ART procedure.

The third procedure studied was a perturbation approach which does not involve iteration. Such an approach was originally developed for ultrasonic problems by Norton and Linzer. It assumes that the index of refraction at each point varies only slightly from its value in the surroundings and that the ray trajectory deviates very little from a straight line. We modified the original analysis to properly represent data acquisition by holographic interferometry including an imaging system. This results in a very simple computation. We found

that both the the SLIM and CRAI techniques tend to initially converge to a more accurate estimated reconstruction and then diverge. Through our study we gained some understanding of the causes of this divergence. We also found that although the CRAI approach is more difficult to implement and slower than SLIM, it is to be preferred in that it generally produces less pronounced divergence.

The primary conclusion drawn from this work, however, is that under most circumstances the simple perturbation technique performs admirably. Particularly in the case of aerodynamic flows where strong divergence from straight optical paths is usually small, this would appear to be the method of choice.

4. PUBLICATIONS

4.1 Journal Articles

1. C. M. Vest, "Tomography for Properties of Materials that Bend Rays: A Tutorial", Applied Optics 24, 4089-4094 (1985).
2. I. H. Lira and C. M. Vest, "Perturbation Correction for Refraction in Interferometric Tomography", Applied Optics, 26, 774-776 (1987).
3. I. H. Lira and C. M. Vest, "Refraction Correction in Holographic Interferometry and Tomography of Transparent Objects", Applied Optics 26, 3919-3928 (1987).
4. D. W. Watt and C. M. Vest, "Digital Interferometry for Flow Visualization", Experiments in Fluids 5, 401-406 (1987).
5. D. W. Watt and C. M. Vest, "Consistent Iterative Convolution: A Coupled Approach to Tomographic Reconstruction" (in preparation, 1987).
6. D. W. Watt and C. M. Vest, "Measurements of Turbulent Jets by Digital Interferometry and Computer Tomography" (in preparation, 1987).

4.2 Doctoral Dissertations

1. I. H. Lira, "Correcting for Refraction Effects in Holographic Interferometry of Transparent Objects", Ph.D. Thesis, The University of Michigan (1987).
2. D. W. Watt, "Turbulent Flow Field Visualization with Integral Interferometric Imaging and Computed Tomography, Ph.D. Thesis, The University of Michigan (1987).

4.3 Presentations at Technical Meetings

1. D. W. Watt and C. M. Vest, "Quasi-heterodyne holographic interferometry for flow visualization", paper TUS7, 1985 Annual Meeting of the Optical Society of America, Washington, D. C., December 1985.
2. I. H. Lira and C. M. Vest, "Tomography of mildly refracting media by interferometry and perturbation analysis", paper TUS6, 1985 Annual Meeting of the Optical Society of America, Washington, D. C., 1985.
3. D. W. Watt and C. M. Vest, "Digital interferometry for flow visualization in the presence of gross periodic noise", paper MW8, 1986 Annual Meeting of the Optical Society of America, Seattle, WA, 1986.

4.4 Reports

C. M. Vest, Progress Reports to ARO covering the following periods:

- 1 January 1984 - 30 June 1985
- 1 July 1985 - 31 December 1985
- 1 January 1986 - 30 June 1986
- 1 July 1986 - 31 December 1986
- 1 January 1987 - 30 June 1987.

5. PARTICIPATING SCIENTIFIC PERSONNEL

Dr. C. M. Vest, Professor, Principal Investigator

Mr. Ignacio H. Lira, doctoral student

Mr. David W. Watt, doctoral student

Both Ignacio Lira and David Watt completed doctoral theses under the sponsorship of ARO through this contract.

APPENDIX

This appendix contains copies of journal articles based on this research which have been published to date. Two more comprehensive articles are in preparation.

Tomography for properties of materials that bend rays: a tutorial

Charles M. Vest

When tomography is performed with electromagnetic or acoustical radiation, refraction may cause sufficient bending of the probing rays that ordinary reconstruction algorithms, which are based on the assumption of straight rays, do not yield accurate results. The resulting problem of reconstructing the refractive-index distribution of an object from time of flight or optical path length data is nonlinear. Various approaches to solving this problem approximately have been proposed and subjected to modest numerical studies. These include iterative algorithms and techniques based on linearized inverse scattering theory. One exception is the case of axisymmetric objects for which an exact solution is known.

I. Introduction

The classical technique of computed tomography is based on the assumption that the probing or emitted rays of radiation are straight lines. This assumption leads to the now well-known problem of reconstruction of some density function from experimentally collected values of its line integrals. This problem is linear and can be approached with the mathematics of the Radon transform and associated techniques. Here we are concerned with cases where the probing or emitted rays are bent by refraction associated with gradients of speed (refractive index) within the object. Hence the density function must be reconstructed from measured values of path integrals along generally unknown curved paths. This problem is inherently nonlinear and is not generally associated with known mathematical transforms.

In this brief tutorial paper, I will discuss several aspects of the problem of computed tomography of objects that bend rays and will outline some of the approaches which have been taken to reconstruct such objects. These problems are associated primarily with ultrasonic and optical tomography. In most applications of tomography using x rays and nuclear sources, the wavelengths are too small for such phenomena to be important. My use of the term rays in the title and

Sec. I displays a personal tendency to think about the problem in terms of ray optics. Other approaches summarized herein are based on wave theory and inverse scattering.

In applications to both ultrasonics and optics (or other domains of electromagnetics), the objective usually is to reconstruct either the distribution of an attenuation (or emission) coefficient or of refractive index. In the case of ultrasonics the measured data are time of flight, intensity, or complex amplitude (real amplitude and phase). In the case of optics the measured data are complex amplitude or intensity. The intensity may in fact be a fringe pattern when the data are gathered interferometrically.

Particularly in the case of ultrasonics, refraction may cause secondary problems—if one is measuring attenuation, refraction can cause divergence of the beam as it travels from the transmitter to the receiver, thereby giving rise to an apparent attenuation. Such problems are compounded if the signal detection is phase sensitive, because phase cancellation effects can occur. Problems of this class have been studied by several authors, and a variety of approximate correction schemes have been developed; see, for example, Farrell,¹ Pan and Liu,² Klepper *et al.*,³ and Itoh *et al.*⁴

Refractive effects can be distributed continuously throughout the object volume, or they can be discrete, as at an object boundary. For example, Eberhard⁵ has dealt with ultrasonic time-of-flight tomography for nondestructive testing of turbine blades. To overcome errors due to very strong bending of the rays at the object boundary, he encapsulated the blade in a rectangular block of material whose refractive index nearly matched that of the blade. Because of this simple rectangular cross section, an algorithm could

The author is with University of Michigan, Department of Mechanical Engineering & Applied Mechanics, Ann Arbor, Michigan 48109

Received 21 September 1984
0003-6935/85/234089-06\$02.00/0
© 1985 Optical Society of America

easily be developed to correct for the effects of refraction at its boundary.

In this paper, we are primarily concerned with refractive effects that are distributed continuously throughout the object. Data are assumed to be either time of flight or optical path length.

II. Axisymmetric Objects: Reconstruction from Path Length Data

It is useful to consider tomography based on optical path length measurements of axisymmetric objects. This case has an analytical solution under modestly constrained conditions. It, therefore, gives insight into the more general problem. Also, experience with interferometry of axisymmetric objects shows the important role played by the physics of the data gathering method, imaging in this case.

A typical ray traversing a cylindrical object with axisymmetric refractive index distribution $n(r)$ is shown in Fig. 1. If refractive effects were negligible, the rays through this object would be straight lines. We then would measure the optical path length (line integral) of all rays in a given direction, say parallel to the y axis. This path length, which we denote as $\phi(x)$, is given by

$$\phi(x) = 2 \int_x^{r_0} \frac{f(r) r dr}{(r^2 - x^2)^{1/2}}, \quad (1)$$

which is an Abel integral of $n(r)$. The inversion of Eq. (1) is well known:

$$f(r) = -\frac{1}{\pi} \int_r^{r_0} \frac{(d\phi/dx) dx}{(x^2 - r^2)^{1/2}}. \quad (2)$$

Thus by measuring one projection we can reconstruct the refractive-index distribution. Note that this is a linear problem. A large number of numerical algorithms have been devised to approximate this reconstruction when data are discrete.

Now let us return to the case where refraction is strong. By definition, the optical path length of the ray shown in Fig. 1 is

$$\phi = \int n ds, \quad (3)$$

where ds is the differential length of the ray. Although we do not know the ray curve, we do know that it is governed by the ray equation

$$\frac{d}{ds} \left(n \frac{dr}{ds} \right) = \nabla n, \quad (4)$$

which has a simple solution, for the axisymmetric case, termed Bouguer's formula⁶:

$$rn(r) \sin(i) = p \quad (5)$$

Note that the rays are parametrized by the constant, p , sometimes called the impact parameter. By introducing a new variable,

$$\eta = rn(r) \quad (6)$$

together with geometric relations derived from Fig. 1, the following expression for the optical path length can be found:

$$\phi(p) = 2 \int_{r_0}^{r_0} \frac{(nd \ln r) d\eta d\eta}{(n - p)^{1/2}} \quad (7)$$

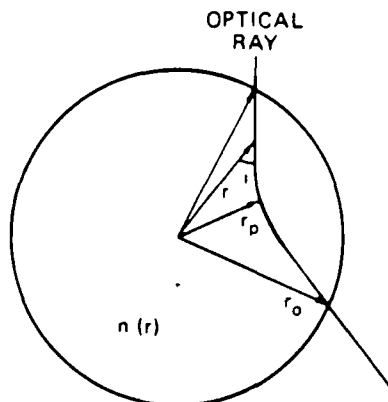


Fig. 1. Optical ray passing through a strongly refracting axisymmetric object.

It is quite interesting to note that although the problem we are solving is highly nonlinear, Eq. (7) is the Abel integral of the quantity $[\eta d \ln(r)/d\eta]$; hence its solution is of the form of Eq. (2):

$$\eta \left(\frac{d \ln r}{d\eta} \right) = -\frac{1}{\pi} \int_{\eta}^{\eta_0} \frac{(d\phi/dp) dp}{(p^2 - \eta^2)^{1/2}}. \quad (8)$$

If desired, this can be integrated to give

$$\frac{r}{r_0} = \exp \left[\frac{1}{\pi} \int_{\eta}^{\eta_0} \cosh^{-1} \left(\frac{p}{\eta} \right) \frac{d\phi}{dp} \frac{dp}{p} \right]. \quad (9)$$

Thus given the set of path integrals and the values of the impact parameter (i.e., the entrance or exit direction and the refractive index at the boundary), the refractive-index distribution is reconstructed implicitly and can be determined as long as the quantity $rn(r)$ is a monotonic function of r . Further discussion of this type of reconstruction can be found in Bullen,⁷ Phinney and Anderson,⁸ and Vest⁹ in the context of geophysical acoustics, radio exploration of planetary atmospheres, and interferometry of gases, respectively.

An interesting effect occurs when axisymmetric strongly refracting objects are studied by interferometry. In this case the data are recorded in the form of a fringe pattern formed by the interference of a reference plane wave with an initially plane wave that has been distorted by travelling through the object. From this fringe pattern one can determine the distribution of phase across the test wave. If the refraction is negligible, all rays involved are essentially straight and parallel to each other. We again have a simple Abel problem which can be solved for $f(r) = n(r) - n_0$, where n_0 is the uniform refractive index of the medium surrounding the object.

Now suppose that the object strongly refracts the test wave, as in Fig. 1. It then is important to introduce an imaging lens between the object and the plane in which the fringe pattern is to be observed. This lens can be focused on any plane parallel to the observation plane. It has been shown by extensive numerical experiments,¹⁰ that if the lens is focused on the center plane of the object, and if one applies the Abel inversion to the data as if no refraction had occurred, the

reconstruction will be very accurate, even if refraction is extremely strong. If another plane, away from the center, is imaged, this procedure will not give a good result. Hence imaging, or an equivalent data processing operation, essentially eliminates the problems associated with strong refraction in interferometry of axisymmetric objects.

III. Asymmetric Objects: Reconstruction from Path Length Data

Consider the data gathering system shown in Fig. 2. It is assumed that the field of interest is two-dimensional and lies in a circular region. Data are collected by interferometry; the fringe pattern is formed in the image plane by an imaging system focused on a plane located a distance r_f from the center of the circle. The unknown refractive-index field is represented by $n(r, \phi)$, the optical axis is aligned so that in the absence of refraction the projection direction would be specified by the angle θ , and the optical path length value is recorded at a point P in the image plane, which is the conjugate of the point P in the object space. As shown in the figure, two rays meet and interfere at point P : one travels a curved path through the object because of refraction due to $n(r, \phi)$, and the other is a reference ray which travels along a straight path through a medium with uniform refractive index n_0 .

Using elementary geometric optics it is seen that the corresponding optical path length difference is given by

$$\begin{aligned} \Delta\tilde{\phi}(p, \theta) &= \int_A^H n(r, \phi) ds + n_0(\overline{BC} - \overline{DE} - \overline{EF}) \\ &= \tilde{P}[n(r, \phi); n_0]. \end{aligned} \quad (10)$$

Cha and Vest¹¹ have termed this the optical path length transform. [Note that if ray bending is negligible, it reduces to the line integral transform, $\Delta\tilde{\phi} = \tilde{P}[n(r, \phi); n_0]$ to which the usual techniques of computed tomography can be applied.] Two approaches have been proposed to obtain reconstructions from data of this general type: iterative algorithms and perturbation analysis. Both take as a starting point an initial reconstruction made by ignoring refraction. To discuss these, a deviation function which is the difference between the path length transform and the line integral transform of the object, or of an estimate of the object, is defined:

$$D(p, \theta) = \Delta\tilde{\phi}(p, \theta) - \Delta\hat{\phi}(p, \theta) \quad (11)$$

The iterative procedure was devised by Cha¹² and is discussed in detail in Ref. 11. The algorithm is as follows:

(i) Make an initial estimate of the deviation function $D(p, \theta)$, where $i = 0$. (Note that we need not start with $D_0 = 0$; if one has some *a priori* knowledge about the general structure of the object, convergence may be speeded by guessing the rough structure of the deviation function.)

(ii) Calculate the corresponding estimate of the line integral transform:

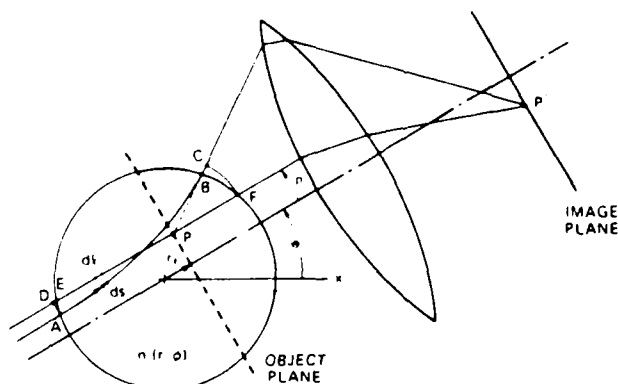


Fig. 2. Formation of an interferogram of an asymmetric refracting object.

$$\Delta\tilde{\phi}_i(p, \theta) = \Delta\hat{\phi}(p, \theta) - D_i(p, \theta). \quad (12)$$

(iii) Reconstruct the object approximately by computing the inverse line integral transform:

$$n_i(r, \theta) - n_0 = \tilde{P}^{-1}(\Delta\tilde{\phi}_i). \quad (13)$$

(iv) Using computational ray tracing,¹³ calculate the path length transform of the estimated distribution:

$$\Delta\tilde{\phi}_i(p, \theta) = \tilde{P}[n_i(r, \phi); n_0]. \quad (14)$$

(v) Compute a new estimate of the deviation function:

$$D_i(p, \theta) = \Delta\tilde{\phi}_i - \Delta\hat{\phi}_i. \quad (15)$$

(vi) Return to step (ii) and continue the process iteratively until some measure of $D_i(p, \theta)$ is sufficiently small.

Cha and Vest¹¹ have applied this algorithm to several numerical experiments in which data computed for a specified object are used as input to the algorithm, and its convergence toward an accurate reconstruction was studied. The algorithm did indeed produce rather accurate reconstructions in the specific cases studied; however, some operator interaction was needed to detect computational ray crossing. Path length data contaminated by this effect were eliminated. They also applied a modified form of this algorithm to experimental data obtained from interferometry from strongly refracting electrochemical boundary layers. Related work on iterative correction for ray bending has been carried out by Greenleaf and Johnson (see, e.g., Ref. 14) and Glover and Sharp.¹⁵

Another iterative approach was developed by Schomberg.¹⁶ He devised a modified ART procedure to determine refractive index at discrete pixels. For each iteration, the coefficients of the algebraic equations are determined by ray tracing using the values of refractive index from the previous iteration. This process is continued until the computed and measured path integrals are in good agreement.

McKinnon and Bates¹⁷ have presented another iterative algorithm that does not require ray tracing at

each iteration. They accomplish this by the less time-consuming task of solving an approximate form of the eikonal equation.

To summarize, several iterative algorithms have been proposed. Each has been demonstrated to produce improved reconstructions in a small number of experiments or numerical simulations. On the other hand, each of these is a somewhat *ad hoc* procedure for which no proof or convincing argument for convergence under general conditions has been given. In fact, McKinnon and Bates¹⁷ indicate that in the common format for recording ultrasonic data, refracting objects have forbidden regions which cannot be reconstructed, and that it may seldom be feasible to improve significantly images beyond those reconstructed by ignoring refraction. Although this may be overly pessimistic in view of some of the successful applications to smoothly varying objects, it is clear that such procedures must be applied with caution, and that more study of convergence and algorithm behavior is needed.

Although iterative procedures are an obvious approach to the problem under consideration, they are inherently slow and expensive because ray tracing is computationally time-consuming. Hence there is motivation to seek more direct approaches. Norton and Linzer¹⁸ have carried out an extensive study of the application of perturbation analysis to the problem of reconstruction of objects that bend rays. In essence, they also start with a deviation function representing the difference between data received from the refracting medium and that which would be received if the probing rays were straight lines. However, they then seek a single operation which can be directly applied to this deviation function to generate an accurate approximate reconstruction.

Because Norton and Linzer's analysis is designed to be applied directly to time-of-flight ultrasonic data with no imaging or interferometry, it is convenient to use their notation, which differs from that above. It is assumed that the ultrasonic refractive index deviates from unity by only a small amount:

$$n(r) = 1 + \epsilon h(r), \quad (16)$$

where $\epsilon \ll 1$ is a small parameter. Correspondingly, as indicated in Fig. 3, the actual ray path \mathcal{L} deviates slightly from the straight path L . If \mathbf{R} is a vector extending from the transmitter T to the receiver R , the time of flight through the object is

$$T_L(\mathbf{R}) = \int_{T, \mathbf{R}} n(r) ds, \quad (17)$$

where the subscript reminds one that this time is associated with the curved path \mathcal{L} , as opposed to the straight path L . Now let $\hat{n}(\mathbf{R})$ be an estimate of the refractive index obtained from a straight line algorithm, i.e., a reconstruction obtained by neglecting refraction,

$$T_L(\mathbf{R}) = \int_{T, \mathbf{R}} \hat{n}(\mathbf{R}) ds. \quad (18)$$

A time-delay correction, or deviation function, is defined as

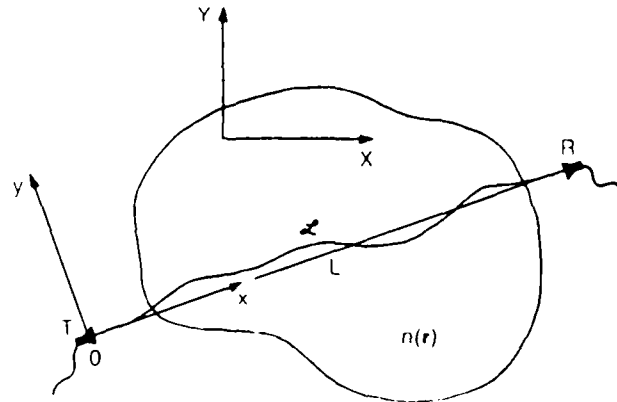


Fig. 3. Ray passing through a mildly refracting object. It originates at transmitter T and impinges on receiver R .

$$e(\mathbf{R}, \hat{n}) = T_L(\mathbf{R}) - T_L(\mathbf{R}). \quad (19)$$

The objective of this technique is to derive a directly calculable expression for $e(\mathbf{R}, n)$.

Because the ray path is assumed to deviate only slightly from the straight line L , and because the refractive index along \mathcal{L} differs only slightly from that along the line, each can be expanded in power series in the perturbation parameter ϵ as

$$y(x) = \epsilon f(x) + O(\epsilon^2) \quad (20)$$

and

$$n(x, y) = 1 + \epsilon h_0(x) + \epsilon^2 f(x) h_1(x) + \dots, \quad (21)$$

where $y(x)$ is the trajectory of the ray passing through O and R and where

$$h_0(x) = h(x, 0), \quad h_1(x) = (\partial h / \partial y)|_{y=0}. \quad (22)$$

By applying Fermat's principle and the calculus of variations, Norton and Linzer¹⁸ minimize T_L with respect to $y(x)$ and obtain the explicit expression for the deviation function e :

$$e = \epsilon^2 \int_0^1 \left(f h_1 + \frac{1}{2} f^2 \right) dx, \quad (23)$$

where $f(x)$ is the solution of

$$d^2 f / dx^2 = h_1(x) \quad (24)$$

subject to

$$f(0) = f(1) = 0. \quad (25)$$

There are several assumptions which must be considered if one wishes to apply this technique. First and foremost, because it is based on a perturbation analysis, variations of refractive index must be small. Numerical simulations suggest that velocity variations should be limited to about $\pm 5\%$, which suggests, for example, that it should be applicable to soft tissue measurements. Variations of refractive index also should be smooth. The application of ray optics must be appropriate, and the transducer width w should be sufficiently small:

$$\sqrt{|u|} \ll a, \quad (26)$$

where a is the characteristic scale of the inhomogeneities of refractive index, and l is the propagation distance across the object.

IV. Methods Based on Diffraction and Inverse Scattering Theory

Rather than utilizing a ray-optical approach, it is possible to view reconstruction of refractive index as a problem in inverse scattering theory. If diffraction is mild, this can be approached by using the Rytov or Born approximations to the wave equation. Iwata and Nagata¹⁹ first applied this approach to problems of reconstruction from optical data in 1975. Kenue and Greenleaf²⁰ recently considered the use of the Rytov approximation for reconstruction from ultrasonic time-of-flight data. Their approach is briefly outlined below.

Figure 4 depicts a plane wave of radiation impinging on the object $f(x,y)$ of interest and being refractively distorted as it propagates through it. At some plane beyond the object the complex amplitude

$$U(\mathbf{r}) = \exp[iK_0\phi(\mathbf{r})] \quad (27)$$

of the emerging wave is measured in an observation plane. This is repeated for a number of different propagation directions. It is assumed that the Helmholtz wave equation applies:

$$\nabla^2 U(\mathbf{r}) + [K_0 n(\mathbf{r})]^2 U(\mathbf{r}) = 0. \quad (28)$$

The eikonal then must obey the relation

$$iK_0^{-1}\nabla^2\phi - (\nabla\phi)^2 + n^2 = 0. \quad (29)$$

Remembering that the variation or refractive index $n(\mathbf{r})$ is small, it is appropriate to write

$$n = 1 + n_1, \quad \phi = \phi_0 + \phi_1, \quad (30)$$

where ϕ_0 is the eikonal in the undisturbed medium. For the entering plane wave,

$$\phi_0 = \mathbf{K} \cdot \mathbf{R}. \quad (31)$$

Integrating across the object we obtain the line integral

$$\phi_k - \phi_a = \int_a^{(b-a)} n_1(x,y) ds. \quad (32)$$

When Eq. (30) is substituted into Eq. (29), we obtain to first order

$$\nabla^2\phi_1 + K_0^2\phi_1 = i2K_0n_1 \quad (33)$$

For a fixed frequency K_0 and direction θ , the 2-D Fourier transform solution of this equation is

$$\hat{n}(U,V) = iu/2\pi K_0 \exp[iu(X_0 - u)X_0] \hat{\phi}_1(X_0, v, 0), \quad (34)$$

where u and v are the transform variables in the direction of \mathbf{K} and normal to \mathbf{K} , respectively.

The complex log of the measured values of $U(\mathbf{r})$ is calculated to give ϕ_1 , whose 1-D Fourier transform is then computed and substituted into Eq. (34). This gives the 2-D transform along a circle in the 2-D transform plane. Note that to obtain values around the

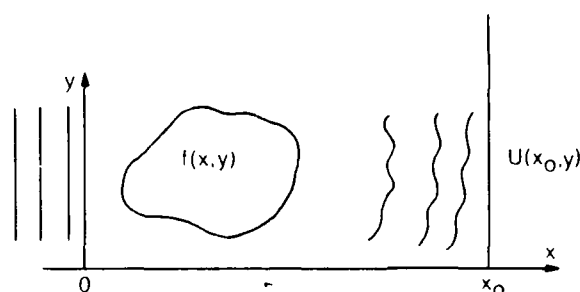


Fig. 4. Complex amplitude of a wave (initially plane) that has propagated through a refracting object.

entire circle requires both transmission and reflection data. If this is repeated for several different propagation directions, the entire Fourier transform plane can be filled in. The refractive-index distribution can then be computed by inverse transformation.

It is interesting to note the analogy between the above result and the central section theorem of ordinary computed tomography.

Recent work by Devaney^{21,22} has treated this type of inverse problem for weakly scattering objects using the Born approximation. Again the fundamental result is that by computing 1-D Fourier transforms of the complex amplitude of the scattered field it is possible to determine the 2-D transform of the object's refractive index along circular arcs. He has generated a filtered backpropagation algorithm that operates in a manner somewhat analogous to the well-known filtered backprojection algorithm of ordinary computed tomography. This interesting and important technique is discussed in a paper by Devaney.²³

V. Closure

In this paper I have outlined some of the techniques which have been proposed for reconstruction of refracting and diffracting objects from data obtained in a manner analogous to ordinary computed tomography. Emphasis has been on cases where time of flight or optical path length data are recorded for radiation passing through a continuous refracting object. Because this problem is nonlinear it has been approached by iterative schemes or by linearized inverse scattering theory. Only a few empirical studies of these approaches have been carried out to date. Although some of these studies have been successful, there is much to be learned about their convergence behavior, reliability, etc. The subject is challenging, interesting, and of potential importance in applications ranging from plasma diagnostics to medical ultrasonic imaging.

Readers should note that I have not discussed closely related topics such as electromagnetic and seismic geophysical exploration^{24,25} or addressed the related problem of refractive errors in ultrasonic tomography based on attenuation measurements.

I would like to thank Richard Gordon for suggesting this review and for helpful comments. This work was sponsored in part by the U.S. Army Research Office.

This paper was presented at the symposium on Industrial Applications of Computed Tomography and NMR Imaging, 13-14 Aug. 1984, Hecla Island, Manitoba, Canada.

References

1. E. J. Farrell, "Tomographic Imaging of Attenuation with Simulation Correction for Refraction," *Ultrason. Imaging* **3**, 144 (1981).
2. K. M. Pan and C. N. Liu, "Tomographic Reconstruction of Ultrasonic Attenuation with Correction for Refractive Errors," *IBM J. Res. Dev.* **25**, 71 (1981).
3. J. R. Klepper, G. H. Brandenburger, J. W. Mimbs, B. E. Sobel, and J. G. Miller, "Application of Phase-Insensitive Detection and Frequency-Dependent Measurements to Computed Ultrasonic Attenuation Tomography," *IEEE Trans. Biomed. Eng.* **BME-28**, 186 (1981).
4. T. Itoh, J.-S. Choi, C. Ksai, and M. Nakajima, "Correction for Refraction on Ultrasonic CT," *Jpn. J. Appl. Phys.* **21**, 149 (1981).
5. J. W. Eberhard, "Quantitative Imaging in Nondestructive Evaluation (NDE) by Ultrasonic Time-of-Flight (TOF) Tomography," *Mater. Eval.* **68** (1982).
6. M. Born and E. Wolf, *Principles of Optics* (Pergamon, New York, 1964), Chap. 6.
7. K. E. Bullen, *An Introduction to the Theory of Seismology* (Cambridge U. P., New York, 1963).
8. R. A. Phinney and D. L. Anderson, *J. Geophys. Res. Space Phys.* **73**, 1819 (1968).
9. C. M. Vest, "Interferometry of Strongly Refracting Axisymmetric Objects," *Appl. Opt.* **14**, 1601 (1975).
10. G. P. Montgomery, Jr., and D. L. Reuss, "Effects of Refraction on Axisymmetric Flame Temperatures Measured by Holographic Interferometry," *Appl. Opt.* **21**, 1373 (1982).
11. S. Cha and C. M. Vest, "Tomographic Reconstruction of Strongly Refracting Fields and its Application to Interferometric Measurement of Boundary Layers," *Appl. Opt.* **20**, 2787 (1981).
12. S. Cha, "Reconstruction of Strongly Refracting Asymmetric Fields from Interferometric Measurements," *Doctoral Dissertation*, U. Michigan, Ann Arbor (1980).
13. A. H. Andersen and A. C. Kak, "Digital Ray Tracing in Two-Dimensional Refractive Fields," *J. Acoust. Soc. Am.* **72**, 1593 (1982).
14. J. F. Greenleaf, S. A. Johnson, and A. H. Lent, "Measurement of Spatial Distribution of Refractive Index in Tissues by Ultrasonic Computer Assisted Tomography," *Ultrasound Med. Bio.* **3**, 327 (1978).
15. G. H. Glover and J. C. Sharp, "Reconstruction of Ultrasound Propagation Speed Distributions in Soft Tissue: Time-of-Flight Tomography," *IEEE Trans. Sonics Ultrason.* **SU-24**, 229 (1977).
16. H. Schomberg, "An Improved Approach to Reconstructive Ultrasound Tomography," *J. Phys. D.* **11**, L181 (1978).
17. G. C. McKinnon and X. Bates, "A Limitation on Ultrasonic Transmission Tomography," *Ultrason. Imaging* **2**, 48 (1980).
18. S. J. Norton and M. Linzer, "Correcting for Ray Refraction in Velocity and Attenuation Tomography: A Perturbation Approach," *Ultrason. Imaging* **4**, 201 (1982).
19. K. Iwata and R. Nagata, "Calculation of Refractive Index Distribution from Interferograms Using the Born and Rytov's Approximation," *Jpn. J. Appl. Phys.* **14-1**, 379 (1975).
20. S. K. Kenue and J. F. Greenleaf, "Limited Angle Multifrequency Diffraction Tomography," *IEEE Trans. Sonics Ultrason.* **SU-29**, 213 (1982).
21. A. J. Devaney, "Inverse Scattering as a Form of Computed Tomography," *Proc. Soc. Photo-Opt. Instrum. Eng.* **358**, 10 (1982).
22. A. J. Devaney, "A Filtered Backpropagation Algorithm for Diffraction Tomography," *Ultrason. Imaging* **4**, 336 (1982).
23. A. J. Devaney, "Coherent Optical Tomography," in *Technical Digest, Topical Meeting on Industrial Applications of Computed Tomography and NMR Imaging* (Optical Society of America, Washington, D.C., 1984), paper TuD3.
24. R. D. Radcliff and C. A. Balanis, "Electromagnetic Geophysical Imaging Incorporating Refraction and Reflection," *IEEE Trans. Antennas Propag.* **AP-29**, 288 (1981).
25. R. J. Lytle and K. A. Dines, "Iterative Ray Tracing Between Boreholes for Underground Image Reconstruction," *IEEE Trans. Geosci. Remote Sensing* **GE-18**, 234 (1980).

Reprinted from *Applied Optics*, Vol. 26, Page 774, March 1, 1987
Copyright © 1987 by the Optical Society of America and reprinted by permission of the copyright owner.

Perturbation correction for refraction in interferometric tomography

Ignacio H. Lira and Charles M. Vest

When this paper was done both authors were with University of Michigan, Department of Mechanical Engineering and Applied Mechanics, Ann Arbor, Michigan 48109; I. H. Lira is now with Pontificia Universidad Católica de Chile, Escuela de Ingeniería, Santiago, Chile.

Received 23 July 1986.

0003-6935/87/050774-03\$02.00/0.

© 1987 Optical Society of America.

Tomographic reconstruction of a function from the values of its line integrals is a well-known diagnostic technique for use in various fields.¹ Several reconstruction algorithms have been developed with the assumption that the probing radiation propagates along straight lines. However, if refractive-index gradients normal to the direction of wave

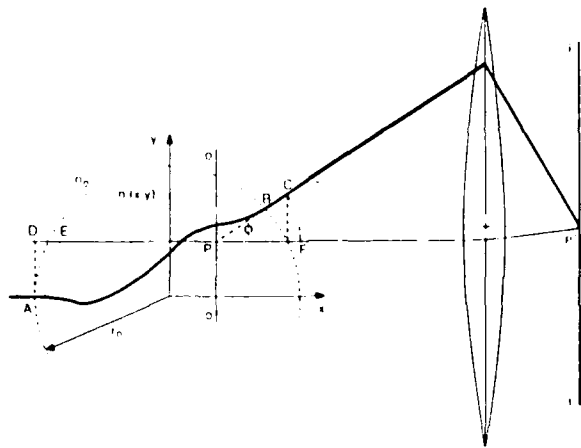


Fig. 1. Schematic representation of the formation of an interferogram with appreciable ray bending. Ray *DEFP*: first exposure, taken with the index of refraction n_0 uniform everywhere. Ray *ABCP*: second exposure, taken with an object of unknown index of refraction $n(x,y)$ varying inside a circular zone of radius r_0 . Imaging system focuses on plane $o-o$.

propagation cause significant ray bending, the use of straight line inversion algorithms may lead to unsatisfactory reconstructions. Ways to correct for refraction effects have been the subject of active research,²⁻⁹ and, at present, this phenomenon may be taken into account through the iterative use of lengthy digital ray tracing algorithms.²⁻⁵ Alternatively, a perturbation technique is available which does not require the use of computational ray tracing. This approach was originally developed by Norton and Linzer⁹ for use in ultrasonic imaging. In this Letter we present a modification of that technique, applicable to holographic and Mach-Zehnder interferometry of transparent objects.

Figure 1 is a schematic representation of the formation of an interferogram by two initially parallel plane waves. It is assumed that outside the circular region, and throughout during one of the exposures, the index of refraction has the uniform value n_0 . The unrefracted ray *DEFP*, representative of that exposure, interferes with ray *ABCP*, which goes through the object. The lens in Fig. 1 is focused on the object plane $o-o$. Point *P* in that plane is the apparent origin of both rays. Point *C* is defined on the refracted ray so that its x coordinate is equal to that of the unrefracted ray at the point where it leaves the test section. Point *F* is defined on the unrefracted ray so that distances \overline{PC} and \overline{PF} are equal. The optical pathlength difference (OPD) between the two rays is given by

$$\Delta\Phi = \int_A^F n ds - n_0(x_F - x_D), \quad (1)$$

where n is the unknown index of refraction of the object and where, if G is a generic point in Fig. 1, x_G denotes its x coordinate. Suppose there was no refraction. Then the OPD would be

$$\Delta\Phi = \int_{r_E}^{r_C} (n - n_0) dx, \quad (2)$$

where E is the point at which both rays enter the test section. Following Norton and Linzer,⁹ we now determine a relation between $\Delta\Phi$ and $\Delta\hat{\Phi}$.

Assume that the index of refraction deviates only slightly from the ambient:

$$n(x,y) = n_0 + \epsilon h(x,y),$$

where ϵ is a small parameter. Assume also that the curved trajectory can be expressed as a small perturbation of a straight line:

$$y = y_P [1 + \epsilon f(x)], \quad (3)$$

where y_P is the y coordinate of point *P*. If the function $h(x,y)$ is expanded about the line $y = y_P$ and if we use Eq. (3), an approximation to the value of the index of refraction along the ray trajectory is obtained. Substitution of this approximation into Eq. (1) and use of Eq. (2) yield, after some rearrangement,⁹

$$\Delta\Phi = \Delta\hat{\Phi} - c,$$

where

$$c = \int_{x_E}^{x_C} \epsilon^2 y_P^2 (f h_y^2 + \frac{1}{2} n_0 y_P f'^2) dx - n_0(x_F - x_C)$$

and where h_y^2 denotes the partial derivative of $h(x,y)$ with respect to y evaluated at $y = y_P$.

Norton and Linzer⁹ obtained an expression for $f(x)$ by using Fermat's principle to minimize the integral $\int_A^C n ds$ and using standard techniques from the calculus of variations. The result is

$$f(x) = \frac{1}{n_0 y_P} \left[\int_{x_E}^x (x - \mu) h_y^2(\mu) d\mu + a_1 x + a_2 \right].$$

The integration constant a_1 is easily evaluated by noting that $f'(x) = 0$ for $x < x_E$, so that $a_1 = 0$. To determine the value of the constant a_2 the following geometric condition is used:

$$\left. \frac{dy}{dx} \right|_{x=x_C} = \frac{y_C - y_P}{x_C - x_P}.$$

After some algebra, the perturbation of the trajectory is found to be

$$f(x) = \frac{1}{n_0 y_P} \left[\int_{x_E}^x (x - \mu) h_y^2(\mu) d\mu - \int_{x_E}^{x_C} (x_P - \mu) h_y^2(\mu) d\mu \right], \quad (4)$$

which differs from the expression developed by Norton and Linzer for ultrasonic imaging because different boundary conditions apply. Equation (4) can now be used to evaluate the term c . Noting from Fig. 1 that

$$x_F - x_C = (x_C - x_P) \left[\frac{1}{\cos(\phi)} - 1 \right],$$

that for small ϕ

$$\frac{1}{\cos(\phi)} - 1 \approx \frac{1}{2} \tan^2(\phi) \approx \frac{1}{2} [\epsilon y_P f'(x_C)]^2$$

and defining

$$H(x) \equiv n_0 [\epsilon y_P f'(x)]^2 = \frac{1}{n_0} \left[\int_{x_E}^x \epsilon h_y^2(\mu) d\mu \right]^2,$$

we obtain

$$c = \frac{1}{2} \left[(x_C - x_P) H(x_C) - \int_{x_E}^{x_C} H(x) dx \right]. \quad (5)$$

The computation of this correction term is based on a first estimate of $n(x,y)$ obtained by straight line inversion of $\Delta\hat{\Phi}$. After c is computed, the modified OPDs are determined and straight line inverted to yield an improved estimate for the index of refraction.

Consider, as an example, a refractive-index distribution of the form

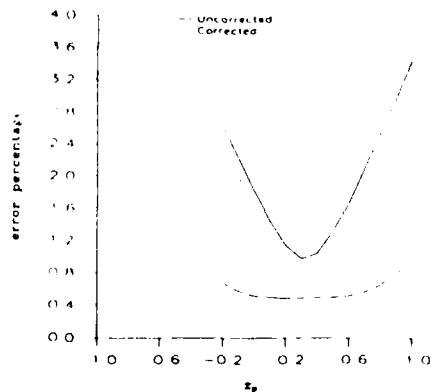


Fig. 2. Root-mean-square error of the uncorrected (solid line) and corrected (dashed line) straight line reconstructions vs object plane selected by the imaging system. The location of the object plane relative to the center of the field is constant for each experiment.

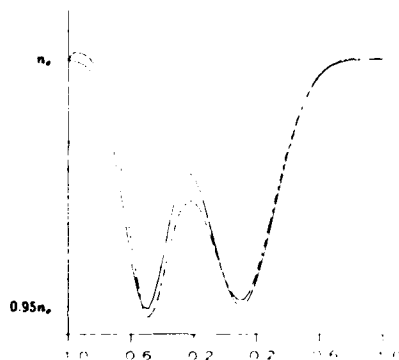


Fig. 3. Cross section of the test field through line $x = 0$. Solid line: actual profile. Dashed line: straight line reconstructed profile. Focusing plane at $x_p = 0.0$.

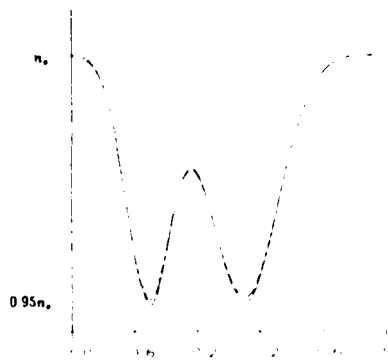


Fig. 4. Cross section of the test field through line $x = 0$. Solid line: actual profile. Dashed line: perturbation corrected profile. Same focusing plane as in Fig. 3.

$$n = 1.0 - 0.05 \exp\left[-\frac{|x^2 + (y - 0.1)^2|}{0.09}\right] - 0.05 \exp\left[-\frac{|x^2 + (y + 0.5)^2|}{0.04}\right]$$

in which the coordinate units are arbitrary. The OPDs were simulated by numerically integrating the ray equation to find the actual ray trajectories through this field. We traced

thirty-two rays per view for each of thirty-two viewing directions. It was found that with $r_0 = 1.0$ the maximum bending angle is 8.5° . To use Eq. (5), x_p needs to be specified. We varied this distance from $-r_0$ to $+r_0$ and kept it constant for each computational experiment. For all reconstructions we used the well-known filtered-backprojection algorithm¹⁰ on a 40×40 grid. The root mean square error of the reconstruction is defined as

$$e = \frac{100}{\max |n_{ie} - n_d|} \sqrt{\frac{1}{m} \sum_{i=1}^m (n_{ie} - n_{ir})^2},$$

where n_{ie} is the exact value of the field in pixel i , n_{ir} is the reconstructed value in that same pixel, and m is the total number of pixels. The error resulting from reconstructions ignoring refraction is the solid line in Fig. 2. No results are shown for $x_p < -0.2r_0$ as ray crossing occurred beyond that position of the object plane. After the perturbation correction for refraction is applied, the error, as shown by the dashed line in Fig. 2, decreases significantly.

Another way to visualize the performance of this method is to compare a cross section of the reconstructed refractive-index profiles. This has been done in Figs. 3 and 4, for which we have chosen $x_p = 0$. In those figures the actual profile is the solid line, while the dashed line is the reconstructed profile. Figure 3 shows the result of the reconstruction ignoring refraction. It can be seen that the corrected reconstruction shown in Fig. 4 is much closer to the actual profile.

If the index of refraction varies along one space coordinate only, as in a boundary layer, the above equations reduce to a much simpler form. Details and an example for this case will appear in a forthcoming paper.

This work was presented at the OSA Annual Meeting, Washington, DC, Oct. 1985. This research is sponsored by the Army Research Office.

References

1. See, e.g., review articles in Proc. IEEE 71, No. 3 (1983) and in Appl. Opt. 24, No. 23 (1985).
2. S. Cha and C. M. Vest, "Tomographic Reconstruction of Strongly Refracting Fields and its Application to Interferometric Measurement of Boundary Layers," Appl. Opt. 20, 2787 (1981).
3. H. Schomberg, "An Improved Approach to Reconstructive Ultrasound Tomography," J. Phys. D 11, L181 (1978).
4. R. J. Lytle and K. A. Dines, "Iterative Ray Tracing between Boreholes for Underground Image Reconstruction," IEEE Trans. Geosci. Remote Sensing GE-18, 234 (1980).
5. S. A. Johnson *et al.*, "Reconstruction of Material Characteristics from Highly Refraction Distorted Projections by Ray Tracing," in *Image Processing for 2-D and 3-D Reconstruction from Projections: Theory and Practice in Medicine and Physical Sciences*, R. Gordon, Ed., A Digest of Technical Papers presented at a Topical Meeting of OSA, Stanford U., Stanford, CA (1975).
6. G. J. Tallents, "Interferometry and Refraction Measurements in Plasmas of Elliptical Cross-Section," J. Phys. D 17, 721 (1984).
7. C. M. Vest, "Interferometry of Strongly Refractive Axisymmetric Phase Objects," Appl. Opt. 14, 1601 (1975).
8. C. M. Vest, "Tomography for Properties of Materials that Bend Rays: a Tutorial," Appl. Opt. 24, 4089 (1985).
9. S. J. Norton and M. Linzer, "Correcting for Ray Refraction in Velocity and Attenuation Tomography: a Perturbation Approach," Ultrason. Imaging 4, 201 (1982).
10. G. N. Ramachandran and A. V. Lakshminarayanan, "Three Dimensional Reconstruction from Radiographs and Electron Micrographs: Application of Convolution Instead of Fourier Transforms," Proc. Natl. Acad. Sci. USA 68, 2236 (1971).

Refraction correction in holographic interferometry and tomography of transparent objects

Ignacio H. Lira and Charles M. Vest

In this paper we review and extend the state of the art in the algorithms that have been developed to tomographically reconstruct 1-D and 2-D refractive-index fields in the presence of significant refraction. A perturbation approach and two iterative procedures were tested and compared in numerical simulation of holographic interferometry experiments. Due to the nonlinearity of the problem, it is very difficult to draw general conclusions with respect to the behavior of the iterative algorithms, which is divergent in the examples presented here. In contrast, the perturbation technique, which is the easiest one to implement and the fastest to run, is shown to be very powerful in reducing refraction errors.

I. Introduction

Inverting the data acquired through holographic interferometry to reconstruct refractive-index fields is a well-established diagnostic technique.¹ By and large, the underlying approximation in the development of the conventional reconstruction algorithms is that the probing radiation travels along a straight line, changing in phase but not in direction, as it crosses the refractive-index inhomogeneities. In reality, when light encounters a refractive-index gradient normal to its direction of propagation, it is refracted. There are many situations in which, for practical purposes, ray bending may be neglected. However, ignoring refraction often produces appreciable reconstruction errors. This has been shown to be the case not only in interferometry² but also in related areas such as geophysical³ and ultrasonic^{4,5} imaging.

Analytical solutions to the highly nonlinear problem of tomographic reconstruction of strongly refracting objects have not been found, so one must resort to computational techniques. In a tutorial paper, Vest² discussed several aspects of the problem and outlined some of the approaches which have been taken to find

an approximate solution. In this paper a more comprehensive and detailed review is presented. In Sec. II we address the 1-D case, which has been considered extensively by previous investigators. Section III discusses the axisymmetric problem, which has also received considerable attention. In Sec. IV the more general 2-D asymmetric problem is considered. Section V contains the results of numerical experiments designed to investigate and compare the performance of the refraction correction schemes. Section VI summarizes the results obtained.

II. One-Dimensional Refractive-Index Fields

We show in Fig. 1 the geometry of the data collection arrangement for the analysis of a 1-D boundary layer using holographic interferometry with plane wave illumination. Above a solid object of length L there is a region with a refractive-index variation of the form $n(y)$ for $y < \delta$. It is assumed that outside the boundary layer, and throughout the entire region during one of the exposures, the index of refraction has the uniform value n_0 . The undeviated ray $DPCP'$, representative of that exposure, interferes with a refracted ray ABP' . The lens in Fig. 1 is focused on the object plane $o-o$. Point P in that plane is the apparent origin of both rays. Point B is the point at which the refracted ray leaves the test section. Point C is defined on the unrefracted ray such that the distance \overline{PC} is equal to the distance \overline{PB} . Due to the presence of the lens, the optical path lengths from B to P' and from C to P' are equal. The optical path length difference (OPD) between the two rays is, then,

$$\Delta\phi_P = \phi_P - \phi_0, \quad (1)$$

where

When this work was done both authors were with University of Michigan, Department of Mechanical Engineering & Applied Mechanics, Ann Arbor, Michigan 48109; I. H. Lira is now with Pontificia Universidad Catolica de Chile, Escuela de Ingenieria, Santiago, Chile.

Received 23 December 1986.

0003-6935/87/183919-10\$02.00/0.

© 1987 Optical Society of America.

$$\Phi_P = \int_A^B n(y) ds,$$

$$\Phi_0 = n_0 x_C,$$

and where x_C is the x coordinate of point C . The subscript in the term Φ_P emphasizes the fact that, to the observer, a fringe located at P' appears to be produced by the interference of two overlapping straight rays through point P . The ray path AB is obtained from the ray equation⁶

$$\frac{d}{ds} \left(n \frac{dr}{ds} \right) = \nabla n, \quad (2)$$

which, in 2-D Cartesian coordinates, reduces to

$$ny'' = \left(\frac{\partial n}{\partial y} - \frac{\partial n}{\partial x} y' \right) [1 + y'^2], \quad (3)$$

where $y = y(x)$ is the path of the ray and the superscripts indicate derivative with respect to x . Using the initial condition $y' = 0$ for $x = 0$ and assuming $n = n(y)$, the integration of this equation gives

$$1 + y'^2 = \left(\frac{n}{n_A} \right)^2, \quad (4)$$

where n_A is the index of refraction at $y = y_A$. Since the ray path element is $ds = \sqrt{1 + y'^2} dx$, the optical path length of the refracted ray through the test section can be expressed as either

$$\Phi_P = n_A \int_0^L (1 + y'^2) dx, \quad (5)$$

or

$$\Phi_P = \frac{1}{n_A} \int_0^L n^2 dx.$$

One of the earliest papers to assess and correct for the influence of refraction was that of Wachtel.⁷ That work was subsequently extended and modified by the research of Howes and Buchele.⁸⁻¹¹ Other papers in which this situation has been considered are Refs. 12-17.

Howes and Buchele¹¹ based their analysis on a Taylor series expansion of the index of refraction around its value at the point where the rays enter the test section, i.e.,

$$n = n_A + \sum_{i=1}^{\infty} b_i (y - y_A)^i. \quad (6)$$

The general analysis¹¹ is quite involved and need not be repeated here. The equations are very simple however, if only two terms in expansion (6) are kept, that is, if

$$n = n_A + n'_A (y - y_A), \quad (7)$$

where n'_A is the derivative of the index of refraction evaluated at $y = y_A$. The ray equation has, in this case, the following exact solution:

$$y = y_A + l_A \left[\cosh \left(\frac{x}{l_A} \right) - 1 \right], \quad (8)$$

where $l_A \equiv n_A / n'_A$. If it can be assumed that $L/l_A \ll 1$,

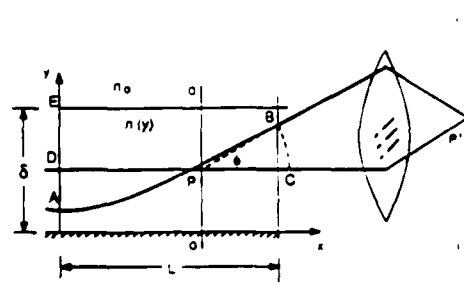


Fig. 1. Interferometric analysis of a 1-D boundary layer-type refractive-index field.

expanding the hyperbolic cosine and keeping only the first two terms in the expansion, Eq. (8) becomes

$$y = y_A + \frac{1}{2} \frac{x^2}{l_A}. \quad (9)$$

To this first level of approximation, then, the ray traces are parabolas. Differentiating Eq. (9) and substituting the result into Eq. (5) give the following approximation for the optical path length of the refracted ray:

$$\Phi_P \approx n_A L \left[1 + \frac{1}{3} \left(\frac{L}{l_A} \right)^2 \right]. \quad (10)$$

On the other hand, from the geometry of Fig. 1 it is readily seen that the optical path length of the unrefracted ray is

$$\Phi_0 = n_0 x_C = n_0 [x_P + (L - x_P) \sqrt{1 + \tan^2 \phi}], \quad (11)$$

where ϕ is the exit angle of the ray. Using Eq. (9), we can approximate the tangent to this angle by

$$\tan \phi \approx \frac{L}{l_A}. \quad (12)$$

Putting this expression into Eq. (11), expanding the square root, and substituting the result, together with Eq. (10), into Eq. (1), we obtain

$$n_A - n_0 \approx \frac{\Delta \Phi_P}{L} - \frac{n_A}{6} \left[2 - 3K \left(\frac{n_0}{n_A} \right) \right] \left(\frac{L}{l_A} \right)^2, \quad (13)$$

where we have defined $K \equiv 1 - x_P/L$.

The index of refraction at $y = y_A$ may now be obtained from Eq. (13) provided n'_A is known. Howes and Buchele suggest that n'_A can be found by differentiating Eq. (13) and assuming that the derivative of the second term on the right-hand side is small compared with that of the first term. Doing this we find

$$n'_A \approx \frac{1}{L} \frac{d \Delta \Phi}{dy} \Big|_{y=y_P}, \quad (14)$$

so that the refractive-index gradient is proportional to the measurable fringe-shift gradient. Alternatively, the effect of the second term can be accounted for by using Eq. (14) as a first approximation to n'_A , substituting this value into Eq. (13), and differentiating again to obtain a refined estimate. This process can be repeated if necessary.

The problem with this method is that the actual entrance coordinates are unknown to the observer. If

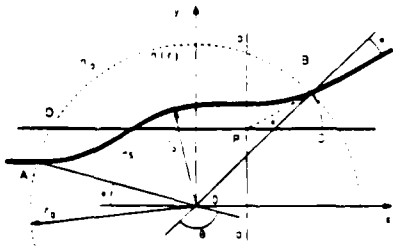


Fig. 2. Schematic representation of the formation of an interferogram in a 2-D axisymmetric refractive-index field.

one uses coordinate y_p , the resulting distribution becomes distorted. Recognizing this problem Howes and Buchele⁸ showed that within the linear approximation the difference $y_p - y_A$ disappears when $K = 1/2$, i.e., when the imaging system is focused at the center of the test section. This can easily be seen to be the case. From Fig. 1 we have

$$\tan \phi = \frac{y_B - y_P}{x_B - x_P} \quad (15)$$

Taking $x_B = L$ and using the parabolic approximation, Eqs. (9) and (12), we find

$$y_p - y_A \approx \frac{L^2}{l_A} \left(\frac{1}{2} - K \right), \quad (16)$$

which verifies the assertion.

In summary, if the linear approximation, Eq. (7), is valid for the range $y_A \leq y_B$, Howes and Buchele recommend using Eq. (13) together with Eq. (14) (with iteration, if necessary) to find $n(y)$. The data should be obtained with the imaging system focused at the center of the test section.

Higher-order refraction correction is possible if more terms in Eq. (6) are included and higher-order derivatives of the fringe order number are calculated. Because the fringes are obtained experimentally, the accuracy of these derivatives becomes increasingly dubious.

A different approach to account for refraction was taken by Svensson.¹⁸ In his analysis he concluded that, with the proper choice of the object plane, the fringe data could be inverted satisfactorily as if no refraction had taken place. Vest¹ simplified Svensson's analysis, but his derivation contains an error in an intermediate step. The correct equations are as follows. Let $\Delta\bar{\Phi}$ be the actual OPD and let $\Delta\Phi$ be the OPD that would be observed if no refraction had taken place. Clearly,

$$\Delta\bar{\Phi}_p = (n_p - n_0)L, \quad (17)$$

but, from Eq. (7),

$$n_p \approx n_1 + n_2(y_p - y_A), \quad (18)$$

Combining Eqs. (17) and (13) and using Eqs. (18) and (16), we find

$$\Delta\bar{\Phi}_p - \Delta\Phi_p = n_2 L \left[\frac{1}{6} - K \left(1 - \frac{n_0}{2n_A} \right) \right] \left(\frac{L}{l_A} \right)^2. \quad (19)$$

Thus, if it can be assumed that $n_0/n_A \sim 1$ throughout the boundary layer, the difference between $\Delta\bar{\Phi}$ and $\Delta\Phi$ is minimized when $K = 1/3$, i.e., when the object plane is chosen to be at a distance of 1/3 of the section length from the window closest to the imaging system. In other words, at that position of the object plane the fringe count may be straight line inverted, as if no refraction had occurred. Note that, contrary to Howes's¹⁹ assertion, minimizing refraction errors in this way does not result in a distorted distribution of the index of refraction. Empirical confirmation of this theory has been given in Ref. 15.

III. Axially Symmetric Refractive-Index Fields

There are many instances of practical importance in which the index of refraction may be considered essentially constant along one direction, while having axial symmetry in a plane perpendicular to that direction. This occurs, for example, when forming interferograms of density in flames, thermal jets, and plumes, or of plasma electron density around exploding wires, arc discharges, or laser beams.

Figure 2 shows a circular test section of radius r_0 being probed by two plane waves. One of them, with representative ray DPC , corresponds to the exposure with uniform index of refraction n_0 everywhere. The other wave, with representative ray AB , corresponds to the exposure taken with the object present, for which the index of refraction is of the form $n(r)$. We assume that during both exposures the index of refraction in the medium outside of the test section has the value n_0 . The imaging system—not shown in the figure—is focused on an object plane $o-o$ located a distance x_p from the center of the field. Point P is the conjugate of the point in the image plane at which both rays interfere.

Kahl and Mylin²⁰ wrote the OPD of these rays in the following form:

$$\Delta\Phi_p = \Phi_p + 2n_0x_A + n_0y_A \tan \phi + n_0x_p(\sec \phi - 1), \quad (20)$$

where $\Phi_p = \int_A^B n(r) ds$ and where the refraction angle ϕ must be taken as positive if the ray bends upward, and negative otherwise. The first two terms on the right-hand side of this equation represent the OPD that would be obtained if no refraction had taken place, the third term is a contribution due to refraction, and the fourth term is an additional focusing effect. Interestingly, this equation shows that all refraction contributions are known if ϕ is known. The OPD given by Eq. (20) is a function of the y_p coordinate given by

$$y_p = y_A \sec \phi + x_p \tan \phi. \quad (21)$$

According to Kahl and Mylin, if a conventional Abel inversion algorithm is used to reconstruct the refractive-index field, it is better to focus on the center of the test section, so that the third contribution in Eq. (20) is eliminated and the difference between the refracted and unrefracted OPDs is kept small. Vest²¹ conducted an extensive computer simulation of interferometric experiments using several analytic functions $n(r)$. All the functions studied had zero slope at $r = 0$ and smoothly approached n_0 at $r = r_0$. He found that Abel

inversion of the actual interferometric data $\Delta\Phi_p$ produces remarkably accurate reconstructions when $x_p = 0$. The above argument explains in part this result. Vest's findings were later confirmed in Refs. 22-24.

In Ref. 21 it is shown that

$$\Phi_p = 2 \int_{r_p}^{r_0} \frac{n^2}{r \sqrt{\eta^2 - p^2}} dr, \quad (22)$$

where $\eta \equiv rn(r)$, $p = n_0 y_A$, and r_p is obtained by solving $\eta(r_p) = p$. In the same reference it is also shown that the angle between OA and OB subtended by the refracted ray is given by

$$\theta = 2 \int_{r_p}^{r_0} \frac{p^2}{r \sqrt{\eta^2 - p^2}} dr. \quad (23)$$

Using the Abel transform, Vest²¹ inverted Eqs. (22) and (23). He found that the index of refraction could be obtained from either

$$r(\eta) = r_0 \exp \left[\frac{1}{\pi} \int_{\eta}^{r_0} \cosh^{-1} \left(\frac{p}{\eta} \right) \frac{1}{p} \frac{d\Phi_p}{dp} dp \right],$$

or

$$r(\eta) = r_0 \exp \left[\frac{1}{\pi} \int_{\eta}^{r_0} \cosh^{-1} \left(\frac{p}{\eta} \right) \frac{d\theta}{dp} dp \right], \quad (24)$$

provided $r(\eta)$ is a single-valued function of radius.

It is easy to show that, if the exponent in Eq. (24) is integrated by parts, the following simpler alternative result is obtained:

$$r(\eta) = r_0 \exp \left[-\frac{1}{\pi} \int_{\eta}^{r_0} \frac{\theta}{\sqrt{p^2 - \eta^2}} dp \right]. \quad (25)$$

The index of refraction can then be obtained from this equation if the central angle θ is known. This result was derived by Maruyama *et al.*²⁵ and independently by Zimin and Frik.²⁶ The former authors recommend the following procedure to find θ . First, obtain the refraction angle ϕ from the derivative of the fringe pattern:

$$\sin \phi = \frac{d\Delta\Phi_p}{dy_p}.$$

Next, calculate the incident angle i_0 by means of the following geometric relation:

$$r_0 \sin i_0 = \sqrt{x_p^2 + y_p^2} \sin \left(\phi + \tan^{-1} \frac{y_p}{x_p} \right).$$

Finally, obtain the central angle from $\theta = \pi - \phi - 2i_0$. Maruyama *et al.* successfully tested this procedure in a simulated experiment in which $n(r)$ was given analytically²⁵ and with an acrylic homogeneous cylinder immersed in a fluid with a slight mismatch in the index of refraction.²⁷

Zimin and Frik,²⁶ manipulating Eq. (25), put it in a form more convenient for calculations. Their result is

$$n(\eta) = n_0 \exp \left[-\frac{1}{\pi} \int_{\eta}^{r_0} \frac{\phi}{\sqrt{p^2 - \eta^2}} dp \right].$$

They used this equation to measure the temperature profile in the thermal boundary layer around a heated

vertical copper cylinder. Comparison with thermocouple measurements gave excellent agreement.

A similar reconstruction procedure was derived by Hunter and Schreiber.²⁸ They showed that the index of refraction can be obtained directly from the fringe-shift data by using the following equation:

$$n(\eta) = n_0 \exp \left[-\frac{1}{\pi} \int_{\eta}^{r_0} \cosh^{-1} \left(\frac{p}{\eta} \right) \frac{1}{p} \frac{d\Delta\Phi_p}{dp} dp \right]. \quad (26)$$

Note that the data are taken as a function of y_p but the derivative is with respect to y_A . However, Hunter and Schreiber tacitly assumed that the apparent and actual entrance coordinates are equal. From the geometry of Fig. 2 it may be seen that this situation will occur for a certain location of the object plane, but this location is not the same for all ray pairs. The applicability of Eq. (26) is therefore restricted to the case in which refraction is very small.

IV. Asymmetric 2-D Fields

We turn now to the more general case of 2-D asymmetric refractive-index fields. This problem has received little attention in interferometry, the only works known to us being the iterative algorithm of Cha and Vest²⁹ and the perturbation approach of Lira and Vest.³⁰ Additionally, another iterative approach has been proposed in the areas of ultrasound tomography^{3,31} and in geophysics^{3,32} but, to our knowledge, it has not been used in interferometry. The techniques are as follows.

A. Straight Line Inversion with Modified Data (SLIM)

This procedure was first introduced in ultrasound tomography by Bates and McKinnon^{33,34} and in interferometry by Cha and Vest.²⁹ Let us first define $\Delta\bar{\Phi}$ as the actual OPD including refraction, obtained by numerical or physical experiment, and $\Delta\bar{\Phi}^k$ as the OPD that would be obtained in a hypothetical experiment involving the same object, but where no refraction occurs. The subscript P has been dropped for conciseness. Cha and Vest's procedure consists of an iterative scheme in which a series of estimates of $\Delta\bar{\Phi}$ are obtained, hopefully converging to its exact unknown value. The algorithm is

$$\Delta\bar{\Phi}^{k+1} = \Delta\bar{\Phi}^k + (\Delta\bar{\Phi} - \Delta\bar{\Phi}^k) \quad \text{with } k = 1, 2, \dots, \quad (27)$$

where $\Delta\bar{\Phi}^k$ is the k th estimate of $\Delta\bar{\Phi}$, n^k is the refractive-index distribution resulting from the straight line inversion of $\Delta\bar{\Phi}^k$, and $\Delta\bar{\Phi}^k$ is the OPD obtained computationally through digital ray tracing³⁵ routines over the field n^k .

It is usually convenient to start by letting $\Delta\bar{\Phi}^1 = \Delta\bar{\Phi}$, i.e., refraction is initially ignored and the data are straight line inverted to yield n^1 . Cha and Vest²⁹ were very successful in applying this technique to 1-D refractive-index fields. However, in two dimensions the results were less conclusive. It was found from numerical simulations that this algorithm will tend to decrease the reconstruction error in the first few iterations, but eventually it diverges.

B. Perturbation Approach

A similar, but computationally much simpler technique, has been presented by Norton and Linzer³⁰ for ultrasonic applications. In their approach it is assumed that the index of refraction differs only slightly from its value at the surroundings and that the ray trajectory deviates very little from the straight line. With these assumptions an improved estimate of $\Delta\Phi$ is obtained and subsequently straight line inverted, without the need for the computational expense of ray tracing and iteration. We³⁰ have modified Norton and Linzer's analysis due to differences between the data acquisition systems used in ultrasonic imaging and in holographic interferometry. Our result is

$$\Delta\Phi \approx \Delta\Phi - c,$$

where

$$c = \frac{1}{2} \left[(x_c - x_p)H(x_c) - \int_{x_g}^{x_c} H(x)dx \right],$$

and where

$$H(x) \equiv \frac{1}{n_0} \left[\int_{x_g}^{x_c} n_y(\mu) d\mu \right]^2.$$

In this expression n_y is the derivative of $n(x,y)$ with respect to y evaluated at $y = y_p$. Points C, E, and P are defined in Fig. 3. The computation of $H(x)$ must be based on a first estimate of $n(x,y)$. As in the SLIM algorithm, this estimate may be obtained by straight line inversion of the actual OPD data $\Delta\Phi$.

If the index of refraction varies along, say, the y coordinate only, the above equations reduce to a much simpler form. Using the points shown in Fig. 1, it is easy to show³⁷ that

$$c = (n_y x_B)^2 \frac{1}{n_0} \left[\frac{1}{3} x_B - \frac{1}{2} x_P \right]. \quad (28)$$

Note that in this case c becomes zero if the object plane is chosen such that $x_P = 2x_B/3$. This result supports the discussion following Eq. (19).

C. Curved Ray Algebraic Inversion (CRAI)

A second iterative technique to obtain the index of refraction, also in the context of ultrasound, was first suggested by Johnson *et al.*⁵ and later by Schomberg.³¹ The basis of this procedure is the utilization of the current estimate of the index of refraction, n^k , to obtain a system of algebraic equations, where the unknowns are the corrections for this estimate at each pixel. Since this technique has not been used in interferometry, we proceed to describe the algorithm in more detail.

The optical path length for a digital ray inside the test section is approximated by

$$\Phi^k \approx \frac{h}{2} n^k(\mathbf{r}_1) + h \sum_{i=2}^{K_i-1} n^k(\mathbf{r}_i) + h_i n^k(\mathbf{r}_{K_i}), \quad (29)$$

where points \mathbf{r}_i with $i = 1, 2, \dots, K_i$ are obtained by digital ray tracing¹⁵ over the field n^k . In this equation subscript i identifies a particular ray and h is the distance between the points. The length h_i depends

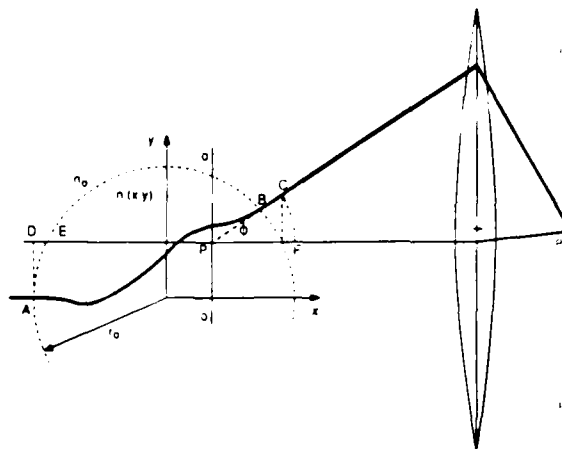


Fig. 3. Schematic representation of the formation of an interferogram in a 2-D asymmetric refractive-index field.

on the location of point \mathbf{r}_{K_i} with respect to the circle boundary. Since in general the points \mathbf{r}_i will not coincide with the pixel centers, interpolation is needed to find the values of the index of refraction at those points. In general, we can write

$$n^k(\mathbf{r}_i) = \sum_{j=1}^m c_{ij}^k n_j^k \quad i = 1, 2, \dots, K_i, \quad (30)$$

where n_j^k is the value of the index of refraction at pixel j in the k th reconstruction and m is the number of pixels. The coefficients c_{ij}^k depend on the interpolation scheme. For example, with bilinear interpolation only the coefficients corresponding to the four nearest pixels are nonzero. Substitution of Eq. (30) into Eq. (29) gives

$$\Phi_i^k \approx \sum_{j=1}^m a_{ij}^k n_j^k, \quad (31)$$

where

$$a_{ij}^k \equiv \frac{h}{2} c_{i1}^k + h \sum_{i=2}^{K_i-1} c_{ij}^k + h_i c_{iK_i}^k. \quad (32)$$

The ray whose optical path is given by Eq. (29) interferes with a straight ray for which an appropriate distance l_i^k must be found, such that

$$\Phi_{0i}^k = n_0 l_i^k. \quad (33)$$

We now form the difference between the optical path lengths given by Eqs. (31) and (33) for several rays in each viewing direction and arrange the result as a vector which we will call $\Delta\Phi^k$. Thus,

$$\Delta\Phi^k = A^k \mathbf{n}^k - n_0 \mathbf{l}^k, \quad (34)$$

where A^k is a matrix whose components are given by Eq. (32), \mathbf{n}^k is a vector formed by the n_j^k pixel values, and \mathbf{l}^k is a vector whose components are the distances l_i^k .

Equation (34) suggests that the actual OPDs can be written as

$$\Delta\Phi = A\mathbf{n} - n_0 \mathbf{l}, \quad (35)$$

where \mathbf{n} is the vector of exact pixel values. Matrix A and vector \mathbf{l} are unknown quantities.

Let us define a correction for the index of refraction as follows: $\delta \mathbf{n}^k \equiv \mathbf{n} - \mathbf{n}^k$. We now substitute this definition into Eq. (35) and assume that $A \approx A^k$ and that $\mathbf{l} \approx \mathbf{l}^k$. If the result is combined with Eq. (34) we obtain

$$A^k \delta \mathbf{n}^k = \Delta \bar{\Phi} - \Delta \bar{\Phi}^k. \quad (36)$$

This system of equations must be solved for the correction $\delta \mathbf{n}^k$, after which the next estimate of the index of refraction is computed according to $\mathbf{n}^{k+1} = \mathbf{n}^k + \delta \mathbf{n}^k$.

We conclude this section by noting that, since Eq. (36) represents a system which will usually be large, sparse, and either under or over determined (depending on the number of rays traced and on the grid size), the solution should be obtained with a series expansion method.³⁸

V. Numerical Experiments

In this section the behavior of the refraction correction algorithms is compared and evaluated by means of computational experiments involving two simple trial functions. Additional results are presented in Ref. 37.

A. Two-Dimensional Example

Consider the following refractive-index field:

$$n(x,y) = n_0 - 0.01n_0 \left\{ \exp - \frac{[x^2 + (y - 0.1)^2]}{0.09} + \exp - \frac{[x^2 + (y + 0.5)^2]}{0.04} \right\}. \quad (37)$$

The OPD data for this double Gaussian distribution was generated using the ray tracing procedure in Ref. 37, with fifty rays for each of twenty viewing directions, spaced 9° apart. If the interferogram is formed using an imaging system focused at the center of the test section, there will be about thirty-six fringes across the object using a He-Ne laser and with the millimeter as the unit of length. This fringe number corresponds to a view in the direction of the y axis. It was found that the maximum bending angle at the exit of the refractive-index field is 1.73° .

In the following study we assumed that the imaging system was kept fixed while the object is rotated about the center, so that the same value of x_p results for all viewing directions.

Figure 4 shows the straight line reconstructed refractive-index profile for $x_p = 2.0$. In this figure the ordinate axis represents the difference $1000 \times (n - n_0)$ in a cross section through the plane $x = 0$, in which the solid line is the exact profile and the dashed line is the reconstruction. The reconstruction error was measured in terms of both the rms and maximum error percentages, defined as

$$e(\text{rms}) = \frac{100}{\max |n_r - n_0|} \sqrt{\frac{1}{m} \sum_{i=1}^m (n_{r,i} - n_{e,i})^2},$$

$$e(\text{max}) = \frac{\max |n_r - n_{e,i}|}{\max |n_r - n_0|} \times 100.$$

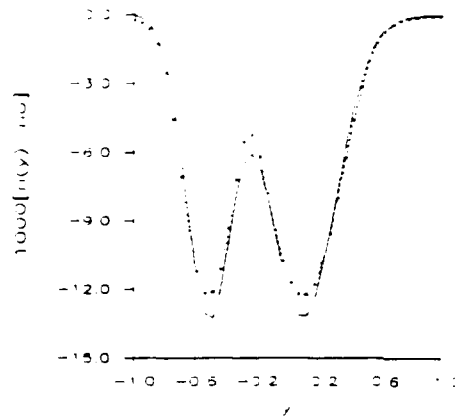


Fig. 4. Straight line reconstructed profile (dashed line) of the double Gaussian distribution compared to the actual profile (solid line). The focusing plane is at $x_p = 2.0$. In obtaining this figure, twenty viewing angles were considered, with fifty rays per view. Resolution is 40×40 pixels. The root-mean square error of this reconstruction is 1.76% and the maximum error is 8.74%.

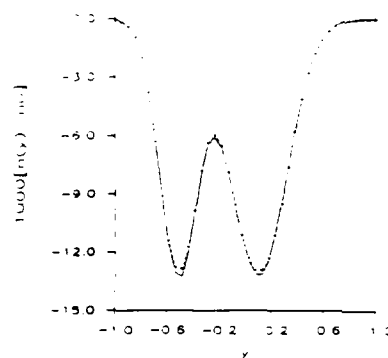


Fig. 5. Perturbation-corrected reconstruction (dashed line) of the double Gaussian distribution compared to the actual profile (solid line). Root-mean square error is 0.35%, maximum error is 2.97%.

where $n_{e,i}$ is the exact value of the field at the center of pixel i , $n_{r,i}$ is the reconstructed value at that same pixel, and m is the number of pixels. For this reconstruction the rms error is 1.76% and the maximum error is 8.74%.

1. Results with the Perturbation Approach

After the perturbation correction is applied, the reconstructed profile looks much closer to the actual profile, as can be observed in Fig. 5. In the corrected profile the rms and maximum errors are 0.35% and 2.97%, respectively, which means a factor of 5 in error reduction. In obtaining these figures, both straight line inversions were done with the filtered backprojection algorithm³⁹ with a Shepp-Logan⁴⁰ filter on a grid of 40×40 pixels.

The quality of the uncorrected reconstruction varies quite significantly as the object plane changes. Figure 6 shows the rms and maximum errors as a function of the object plane. In this figure the solid lines give the errors obtained for the first (uncorrected) reconstruc-

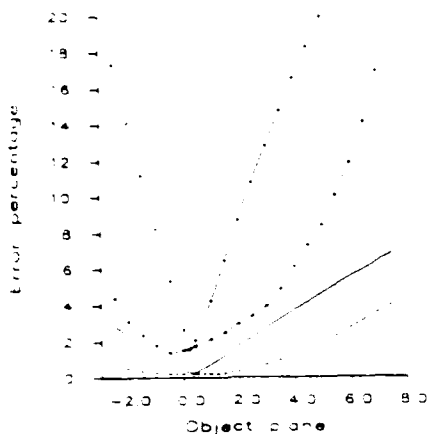


Fig. 6. Reconstruction error as a function of the object plane selected for the straight line (solid lines) and perturbation-corrected (dashed lines) reconstructions of the double Gaussian function. Plain lines give rms errors, while lines with asterisks give maximum errors.

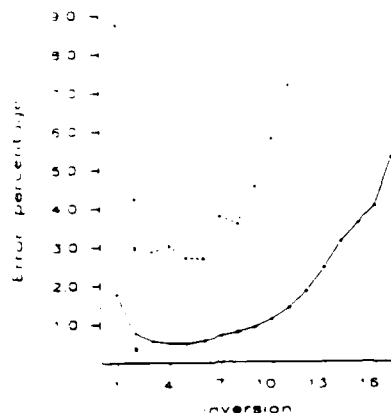


Fig. 7. Reconstruction error as a function of inversion number for the reconstruction of the double Gaussian function using the SLIM iterative approach. The solid line gives the rms error, while the dashed line shows the maximum error. For comparison, the perturbation-corrected errors for the second inversion are shown as white and black symbols for the maximum and rms, respectively. The focusing plane is $x_p = 2.0$.

tion, while the dashed lines are the errors for the inversion obtained after the correction is applied. The plain lines give rms errors, while the lines with asterisks are maximum errors. Results are shown only for $-2.5 < x_p < 7.5$, as ray crossing occurred beyond those positions of the object plane. From this figure it may be seen that the error caused by refraction is almost negligible when the object plane is slightly in front of the center of the field, and that the uncorrected errors are very sensitive to the location of the object plane. In fact, these errors are very nearly directly proportional to the object plane distance from the plane where refraction error is minimized. Thus, to minimize the refraction error the imaging system has to be focused very carefully close to the center of the distribution. The perturbation corrected errors are not as

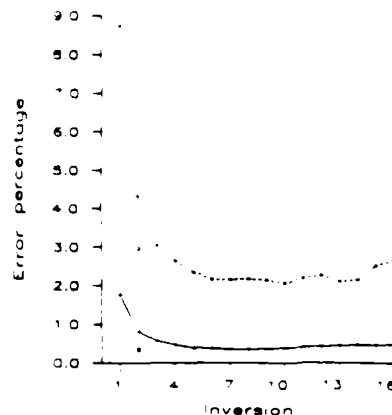


Fig. 8. Reconstruction error as a function of inversion number for the reconstruction of the double Gaussian function using the CRAI. The solid line gives the rms error, while the dashed line shows the maximum error. For comparison, the perturbation-corrected errors for the second inversion are shown as white and black symbols for the maximum and rms, respectively. The focusing plane is $x_p = 2.0$.

sensitive to the object plane location. As Fig. 6 shows, they are almost constant over the range $-2 < x_p < 2$.

2. Results with the SLIM

The SLIM procedure yields the results in Fig. 7. Since this procedure is iterative, it is convenient to show its behavior by plotting the rms and maximum error percentages as a function of the inversion number (where inversion 1 is the first, uncorrected reconstruction) for a given object plane. Space limitations preclude the presentation of equivalent plots for other objects planes. We believe, however, that one object plane should be sufficient to acquire a good idea of the main trends in the behavior of this algorithm. In Fig. 7 the focusing plane has been selected to be $x_p = 2.0$. For direct comparison with the perturbation approach, all results have been obtained using twenty views, fifty rays per view and 40×40 pixels. In this example the SLIM reduces the reconstruction error in the first few iterations, but after inversion 5 the procedure diverges.

3. Results with the CRAI

In the following results we have retained the number of views, the number of rays per view, the grid size, and the focusing plane so that direct comparison between the three approaches can be done. The CRAI algorithm has some additional degrees of freedom, namely, the type of algebraic reconstruction procedure, the number of iterations in that procedure, and the relaxation factor to be used (which may vary from one iteration to the next). In this example the reconstructions were obtained using the SART algorithm of Andersen and Kak⁴¹ with two iterations (i.e., the pixels were updated at the end of the second SART iteration) and a constant relaxation factor of 0.5.

As shown in Fig. 8, the CRAI algorithm yields a mildly unstable solution when reconstructing the dou-

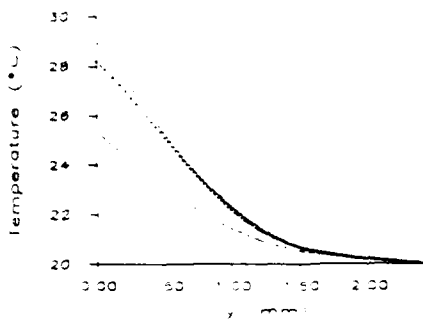


Fig. 9. Temperature distribution in the boundary layer surrounding a heated vertical flat plate submerged in water. Plate temperature is 29°C and ambient water temperature is 20°C. Plate width is 10 cm and the results shown are for a plane 1 cm above the leading edge. In this figure the object plane is at the point where the actual and apparent plate boundaries coincide. The solid curve shows the temperature as given in Ref. 42, using which the interferometric data was generated. The dashed curve shows the temperature obtained with the conventional straight line inversion of the data. The curve with asterisks gives the perturbation-corrected temperature.

ble Gaussian function, diverging after approximately the tenth iteration.

B. One-Dimensional Example

In this subsection the performance of the refraction correction schemes for the case of 1-D ray bending is investigated. The chosen example simulates the refractive-index field resulting from temperature variations in a natural convective boundary layer about a vertical flat plate at 29°C submerged in water at 20°C. The analytic form of this field is given in detail in Ref. 37 and need not be repeated here. Our ray tracing model³⁷ predicts a maximum bending angle of 2.13° for the innermost ray. In this example we have chosen the object plane such that the apparent and actual locations of the wall coincide.

1. Results with the Perturbation Approach

The result of subtracting the correction term as given by Eq. (28) from the OPD data is shown in Fig. 9. In this figure, the solid curve represents the exact temperature profile, the dashed curve represents the temperature obtained using the conventional straight line inversion of the OPD data, and the curve with asterisks gives the perturbation-corrected inversion. There is a very noticeable improvement as a result of applying the correction term.

2. Results with the SLIM

In implementing the iterative algorithms to reduce refraction errors in the 1-D case, the discrete form of the ray tracing routines require the current estimate of the index of refraction in the form of a pixel array in which each entry is the value of the index of refraction at a given y coordinate. Here, and in the next subsection, 50 pixels have been used. Figure 10 shows the rms error and the absolute value of the maximum error for each straight line inversion of the corrected data. The perturbation-corrected errors are also shown in

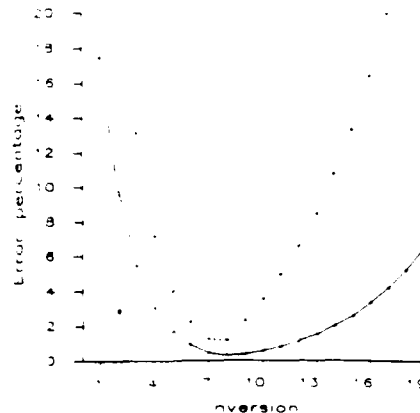


Fig. 10. Reconstruction error as a function of inversion number for the reconstruction of the 1-D temperature profile using the SLIM approach. The solid line gives the rms error, while the dashed line shows the maximum error. For comparison, the perturbation corrected errors for the second inversion are shown as white and black symbols for the maximum and rms, respectively. Percentages are based on 50 pixel values. All other parameters are as in Fig. 9.

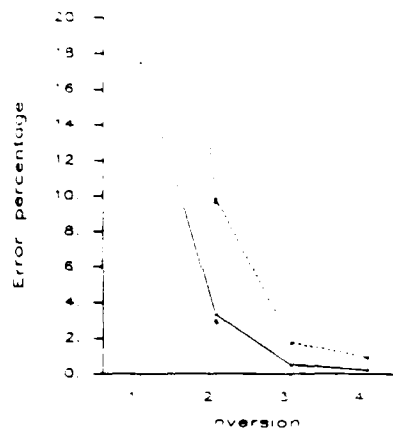


Fig. 11. Reconstruction error as a function of inversion number for the reconstruction of the 1-D temperature profile using the CRAI. The solid line gives the rms error, while the dashed line shows the maximum error. For comparison, the perturbation-corrected errors for the second inversion are shown as white and black symbols for the maximum and rms, respectively. Percentages are based on 50 pixel values. All other parameters are as in Fig. 9.

that figure, as was done in sec. V.A. It is seen in Fig. 10 that the SLIM procedure produces a substantial error decrease up to inversion number eight, but afterward the algorithm diverges.

3. Results with the CRAI

As shown in Fig. 11, the convergence of the CRAI for this example is very fast compared to the SLIM procedure. Thus, at the fourth inversion the errors are 0.22% rms and 0.93% maximum, and the resulting profile practically coincides with the actual one. A small undulation in the reconstructed profile, however, leads to computational ray crossing when we attempt to continue the iterations after the fourth inversion.

VI. Conclusions

Due to the nonlinearity of the problem, it is very difficult to draw general conclusions. From the examples presented above, and from other examples discussed in Ref. 37, it is seen that the quality of the reconstructions and the convergence and divergence characteristics of each algorithm are strongly object-dependent. The most interesting result of this research is the fact that the perturbation technique, which is the easiest one to implement, is quite powerful in reducing refraction errors. This approach has the important advantage of not requiring the use of digital ray tracing, thereby significantly reducing computational costs compared to the iterative procedures. Moreover, it is very appealing since it makes use of straight line inversion, a technique supported by an extensive body of knowledge.

The SLIM algorithm is essentially a less sophisticated attempt to find the difference between actual and unrefracted OPDs. According to Eq. (27), the condition for the convergence of this algorithm is that the difference $\Delta\Phi - \Delta\Phi^k$ must grow progressively smaller. The examples presented here have shown, however, that in some cases that assumption is not correct. To explain this behavior, consider the following argument. Suppose that eventually the exact solution is found, i.e., that for some k we have $n^k \approx n$. Because of discretization and round-off errors, the calculated OPDs $\Delta\Phi^k$ will differ from the exact OPDs $\Delta\Phi$ by a finite amount. The next estimate of the OPDs without refraction, $\Delta\Phi^{k+1}$, will then be different from the ones that produced the correct reconstruction. As a consequence the resulting index of refraction, n^{k+1} , will be different from n . Since this difference is not a product of refraction, it is not likely to be reduced after further iterations.

The CRAI technique for reconstruction along curved rays is based on a totally different approach to the problem. It does not use straight line inversion techniques, and therefore it is more difficult to implement and slower than the SLIM. Nevertheless, we have showed that the CRAI is a very effective technique in correcting for refraction errors. According to Eq. (36), the requirements for the convergence of this algorithm are the same as that for the SLIM. Thus, because numerical errors compound after the minimum error solution is found, the CRAI will also tend to diverge after an acceptable solution has been found. The divergence of the CRAI is, however, usually less pronounced than that obtained with the SLIM.

In conclusion, the evidence presented here suggests that, if refraction becomes non-negligible, the perturbation correction should be applied. For comparison, it may be convenient to use one of the iterative approaches, in which case the CRAI algorithm is recommended. We feel, however, that further research is needed to establish the conditions in which the iterative algorithms will converge or diverge.

References

1. C. M. Vest, *Holographic Interferometry* (Wiley, New York, 1979).
2. C. M. Vest "Tomography for Properties of Materials that Bend Rays: a Tutorial," *Appl. Opt.* **24**, 4089 (1985).
3. R. J. Lytle and K. A. Dines, "Iterative Ray Tracing Between Boreholes for Underground Image Reconstruction," *IEEE Trans. Geosci. Remote Sensing* **GE-18**, 234 (1980).
4. A. H. Andersen and A. C. Kak, "The Application of Ray Tracing Towards a Correction for Refracting Effects in Computed Tomography with Diffracting Sources," *TR-EE 84-14*, School of Electrical Engineering, Purdue U. (1984).
5. S. A. Johnson, J. F. Greenleaf, A. Chu, J. Sjostrand, B. K. Gilbert, and E. H. Wood, "Reconstruction of Material Characteristics from Highly Refraction Distorted Projections by Ray Tracing," in *Technical Digest of Topical Meeting on Image Processing for 2-D and 3-D Reconstruction from Projections: Theory and Practice in Medicine and the Physical Sciences* (Optical Society of America, Washington, DC, 1975), paper TuB2.
6. M. Born and E. Wolf, *Principles of Optics* (Pergamon, New York, 1975).
7. G. P. Wachtel, "Refraction Error in Interferometry of Boundary Layer in Supersonic Flow Along a Flat Plate," Ph.D. Thesis, Princeton U. (1951).
8. W. L. Howes and D. R. Buchele, "A Theory and Method for Applying Interferometry to the Measurement of Certain Two-Dimensional Density Fields," *NACA TN-2693* (1952).
9. W. L. Howes and D. R. Buchele, "Generalization of Gas-Flow Interferometry Theory and Interferogram Evaluation Equations for One-Dimensional Density Fields," *NACA TN-3340* (1955).
10. W. L. Howes and D. R. Buchele, "Practical Considerations in Specific Applications of Gas-Flow Interferometry," *NACA TN-3507* (1955).
11. W. L. Howes and D. R. Buchele, "Optical Interferometry of Inhomogeneous Gases," *J. Opt. Soc. Am.* **56**, 1517 (1966).
12. E. E. Anderson, W. H. Stevenson, and R. Viskanta, "Estimating the Refractive Error in Optical Measurements of Transport Phenomena," *Appl. Opt.* **14**, 185 (1975).
13. K. W. Beach, R. H. Muller, and C. W. Tobias, "Light-Deflection Effects in the Interferometry of One-Dimensional Refractive-Index Fields," *J. Opt. Soc. Am.* **63**, 559 (1973).
14. F. R. McLarnon, R. H. Muller, and C. W. Tobias, "Derivation of One-Dimensional Refractive-Index Profiles from Interferograms," *J. Opt. Soc. Am.* **65**, 1011 (1975).
15. J. M. Mehta and W. Z. Black, "Errors Associated with Interferometric Measurement of Convective Heat Transfer Coefficients," *Appl. Opt.* **16**, 1720 (1977).
16. J. M. Mehta and W. M. Worek, "Analysis of Refraction Errors for Interferometric Measurements in Multicomponent Systems," *Appl. Opt.* **23**, 928 (1984).
17. F. W. Schmidt and M. E. Newell, "Evaluation of Refraction Errors in Interferometric Heat Transfer Studies," *Rev. Sci. Instrum.* **39**, 592 (1968).
18. H. Svensson, "The Second-Order Aberrations in the Interferometric Measurement of Concentration Gradients," *Opt. Acta* **1**, 25 (1954).
19. W. L. Howes, "Rainbow Schlieren vs Mach-Zehnder Interferometer: a Comparison," *Appl. Opt.* **24**, 816 (1985).
20. G. D. Kahl and D. C. Mylin, "Refractive Deviation Errors of Interferograms," *J. Opt. Soc. Am.* **55**, 364 (1965).
21. C. M. Vest, "Interferometry of Strongly Refracting Axisymmetric Phase Objects," *Appl. Opt.* **14**, 1601 (1975).
22. G. Gillman, "Interferometer Focussing Accuracy and the Effect on Interferograms for Density Measurements of Laser Produced Plasmas," *Opt. Commun.* **35**, 127 (1980).

23. G. P. Montgomery, Jr. and D. L. Reuss. "Effects of Refraction on Axisymmetric Flame Temperatures Measured by Holographic Interferometry," *Appl. Opt.* 21, 1373 (1982).
24. D. W. Sweeney, D. T. Attwood, and L. W. Coleman. "Interferometric Probing of Laser Produced Plasmas," *Appl. Opt.* 15, 1126 (1976).
25. Y. Maruyama, K. Iwata, and R. Nagata. "A Method for Measuring Axially Symmetrical Refractive Index Distribution Using Eikonal Approximation," *Jpn. J. Appl. Phys.* 15, 1921 (1976).
26. V. D. Zimin and P. G. Frik. "Strong Refraction by Axisymmetric Optical Inhomogeneities," *Sov. Phys. Tech. Phys.* 21, 233 (1976).
27. Y. Maruyama, K. Iwata, and R. Nagata. "Determination of Axially Symmetrical Refractive Index Distribution from Directions of Emerging Rays," *Appl. Opt.* 16, 2500 (1977).
28. A. M. Hunter II and P. W. Schreiber. "Mach-Zehnder Interferometer Data Reduction Method for Refractively Inhomogeneous Test Objects," *Appl. Opt.* 14, 634 (1975).
29. S. Cha and C. M. Vest. "Tomographic Reconstruction of Strongly Refracting Fields and Its Application to Interferometric Measurement of Boundary Layers," *Appl. Opt.* 20, 2787 (1981).
30. I. H. Lira and C. M. Vest. "Perturbation Correction for Refraction in Interferometric Tomography," *Appl. Opt.* 26, 774 (1987).
31. H. Schomberg. "An Improved Approach to Reconstructive Ultrasound Tomography," *J. Phys. D* 11, L181 (1978).
32. R. D. Radcliff and C. A. Balanis. "Electromagnetic Geophysical Imaging Incorporating Refraction and Reflection," *IEEE Trans. Antennas Propag.* AP-29, 288 (1981).
33. R. H. T. Bates and G. C. McKinnon. "Towards Improving Images in Ultrasonic Transmission Tomography," *Australas. Phys. Sci. Med.* 2-3, 134 (1979).
34. G. C. McKinnon and R. H. T. Bates. "A Limitation on Ultrasonic Transmission Tomography," *Ultrasonic Imaging* 2, 48 (1980).
35. A. H. Anderson and A. C. Kak. "Digital Ray Tracing in Two-Dimensional Refractive Fields," *J. Acoust. Soc. Am.* 72, 1593 (1982).
36. S. J. Norton and M. Linzer. "Correcting for Ray Refraction in Velocity and Attenuation Tomography: a Perturbation Approach," *Ultrasonic Imaging* 4, 201 (1982).
37. I. H. Lira. "Correcting for Refraction Effects in Holographic Interferometry of Transparent Objects," Ph.D. Thesis, U. Michigan (1987).
38. Y. Censor. "Finite Series-Expansion Reconstruction Methods," *IEEE Proc.* 71, 409 (1983).
39. G. N. Ramachandran and A. V. Lakshminarayanan. "Three Dimensional Reconstruction from Radiographs and Electron Micrographs: Application of Convolution instead of Fourier Transforms," *Proc. Natl. Acad. Sci. U.S.A.* 68, 2236 (1971).
40. L. A. Shepp and B. F. Logan. "The Fourier Reconstruction of a Head Section," *IEEE Trans. Nucl. Sci.* NS-21, 21 (1974).
41. A. H. Andersen and A. C. Kak. "Simultaneous Algebraic Reconstruction Technique (SART): a Superior Implementation of the ART Algorithm," *Ultrasonic Imaging* 6, 81 (1984).
42. B. Gebhart and L. Pera. "The Nature of Vertical Natural Convection Flows Resulting from the Combined Buoyancy Effects on Thermal Mass Diffusion," *Int. J. Heat Mass Transfer* 14, 2025 (1971).

MEASUREMENT OF LASER OUTPUT CHARACTERISTICS

Effective use of lasers in technology, manufacturing, defense and energy research requires a precise control of the laser output: spatial, spectral, temporal, energy and power. Ability to specify and/or reliably measure these characteristics with a predictable degree of accuracy is a necessity for those working in laser research development, manufacture, sales, testing and use. Demonstrations and simulated problem sessions are featured to reinforce lecture principles, practice calculations and familiarize the student with laser/optics detection equipment and techniques.

ENGINEERING TECHNOLOGY INSTITUTE
 P. O. Box 8859
 Waco, TX 76714-8559
 (817) 772-0082
 1-800-367-4238

5 Days
 Cost: \$850.00

November 2-6, 1987
 Los Angeles, CA

Digital interferometry for flow visualization *

D. W. Watt and C. M. Vest

Department of Mechanical Engineering, University of Michigan, Ann Arbor, MI 48109, USA

Abstract. Digital holographic interferometry is a hybrid optical-digital technique for determining the phase of an interferogram. This technique improves the accuracy of interferometric measurement of fluid properties and enhances the utility of interferometric flow visualization. Displays of the interferometric phase produce excellent images of weakly refracting two-dimensional flows and can be used to produce integral projection images of three dimensional flows which differ from and complement schlieren and shadowgraph images. The technique is explained herein and examples of its use in both continuous wave and pulsed interferometry are presented.

1 Introduction

Schlieren, shadowgraph and interferometric flow visualization techniques use the integrated effect of a fluid optical property on a beam of light passing through an object to form an image of a flow pattern. These techniques work well for a variety of flows but have limited utility for three-dimensional flows and weakly refracting flows. Schlieren and shadowgraph images are formed by ray bending which is approximately proportional to refractive index gradients and second derivatives of the refractive index, respectively. The latter two techniques work well for two-dimensional flows characterized by large refractive index gradients, such as shock patterns. They also have been used to observe complex structures like turbulent jets. Such images show qualitative flow features such as the gross outline of the motion, the finely grained structure of turbulence (Crow & Champagne 1971), and the presence of large, two dimensional structures [e.g. the vortex-like structures of Brown & Roshko (1974)], but conceal other structural aspects of the flow such as the presence of unmixed, entrained fluid inclusions within the flow.

Interferometric methods are based on the phase delay of a plane wave passing through the object and produce

an integral projection of the object's refractive index field. However, this phase delay is encoded in a fringe pattern which can be difficult to interpret. The fringes are useful for visualizing objects such as plumes and boundary layers, but become complicated for three-dimensional objects. None of these methods works well for weakly-refracting flows because the gradients involved produce indistinct schlieren and shadowgraph images and yield broad, ambiguous interferometric fringes.

Digital interferometry is a technique by which the interferometric phase delay is determined very accurately at a large number of points in the image. The phase may be displayed as a gray scale, yielding an image that has none of the ambiguities associated with Schlieren and shadowgraph images. Furthermore, the technique may be used to image weakly-refracting flows since direct determination of the phase allows one to enhance the contrast of flow details that can not be resolved by conventional interferometry. Finally, the technique may be used to make distributed measurements of flow quantities.

2 Digital interferometry

Digital interferometry is a recently developed hybrid optical-digital metrology technique combining two exposure holographic interferometry with digital image acquisition and computer processing to determine the interferometric phase directly from a set of image irradiance measurements (Dändliker & Thalmann 1985; Hariharan 1985). This technique is similar to heterodyne holographic interferometry in that both manipulate the interferogram's phase in a known manner to determine its magnitude. The image intensity of a holographic interferogram is given by (Vest 1979):

$$I(x, y) = I_0(x, y) \{1 + m(x, y) \cos[\Phi(x, y) + \phi]\} \quad (1)$$

where $I_0(x, y)$ is the background intensity, $m(x, y)$ is the fringe contrast and $\Phi(x, y)$ is the interferometric phase. The term ϕ is the uniform phase bias term which in the

* This work was presented in part at the 1985 Optical Society of America Annual Meeting

case of digital or heterodyne interferometry can be manipulated. The image irradiance is recorded for several different values of this bias phase using a digitizing camera and is stored in computer memory.

The unknown phase Φ can be calculated from the values of the recorded image irradiance distribution and the known values of ϕ using any one of a number of algebraic relationships reviewed recently by Hariharan (1985). In this study, we recorded n separate irradiance patterns with the reference phase ϕ evenly distributed from zero to 2π . The phase Φ may then be determined, modulo 2π by:

$$\Phi(x, y) = \tan^{-1} \frac{\sum_{j=1}^n I_j(x, y) \sin \phi_j}{\sum_{j=1}^n I_j(x, y) \cos \phi_j} \quad (2)$$

where

$$I(x, y) = I_0(x, y) [1 + m(x, y) \cos\{\Phi(x, y) + \phi\}] \quad (3)$$

and $\phi = \frac{2\pi j}{n}$, n = number of exposures. The inverse tan-

gent function maps the fringe pattern into a linear, discontinuous function. This enables one to eliminate the phase sign ambiguity normally associated with cosinusoidal fringes. The usual fringe counting procedure is replaced by a simple, computational sorting operation. A negative discontinuity indicates an increase in fringe number and a positive discontinuity a decrease. Because the phase is evaluated independently at each point in the image, its determination is unaffected by spatial variation in the background irradiance or fringe contrast. The accuracy of phase determination may be of the order of 1/50–1/100 of a fringe, compared with 1/100–1/1,000 of a fringe for heterodyne interferometry and 1/5–1/10 fringe for conventional interferometry, depending in all cases on the nature of the object being studied (Dändliker & Thalmann 1985). The combined use of computational fringe counting and high resolution image storage devices enables one to resolve complex fringe patterns. Digital interferometry is a convenient, accurate high resolution interferometric technique.

This method can be used for both real-time (Hariharan et al. 1982) and double exposure holographic interferometry. Because real-time images show temporal phase variation due to even small perturbations which are inherent in many fluid mechanics experiments, double exposure methods are preferred for most steady flow studies and all unsteady flow studies. The double exposure technique requires two reference waves, one for each exposure (Fig. 1). The first exposure is made without the object (flow field) and the second exposure is made with the object present. The film is developed and the image is reconstructed by illuminating it with both reference waves simultaneously. Primary, conjugate and cross reconstructions are then present (Dändliker et al. 1976). The con-

jugate and cross reconstructions must be properly compensated for so that their presence does not significantly reduce the accuracy of the technique (Dändliker et al. 1982). The two primary reconstructions overlap to form the desired interferogram with the phase bias term given by:

$$\phi = k(r_1 - r_2) - k(r'_1 - r'_2) \quad (4)$$

where $k = \frac{2\pi}{\lambda}$; λ = recording wavelength; r_1, r_2 are the reference source distances during recording, and r'_1, r'_2 are the reference source distances during reconstruction. The phase bias term ϕ may be shifted by changing the path length of either reference wave by a small amount, Δr . Therefore the change in the phase bias term is $\Delta\phi = k\Delta r$.

This technique can be applied to flow visualization or measurement with either plane-wave or diffused object illumination. The plane wave setup (Fig. 2) is preferable when laser power is limited. When a plane object wave is used, the two reference waves must have a wide angular separation in order to eliminate troublesome overlap of the cross reconstructions.

Diffused illumination (Fig. 3) is generally preferable, however, because it allows the two reference waves to have a small angular separation, thereby reducing the errors due to misalignment of the hologram with the two reference waves. Although the cross-reconstructions overlap, they may be almost completely decorrelated if their

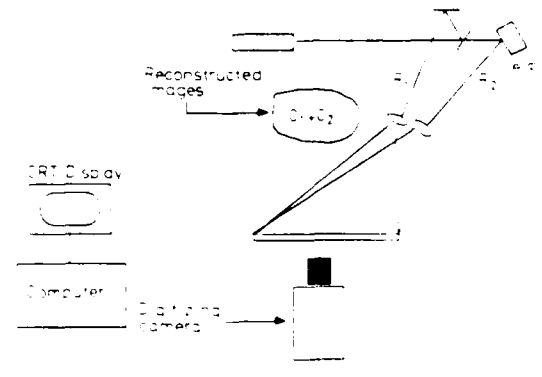
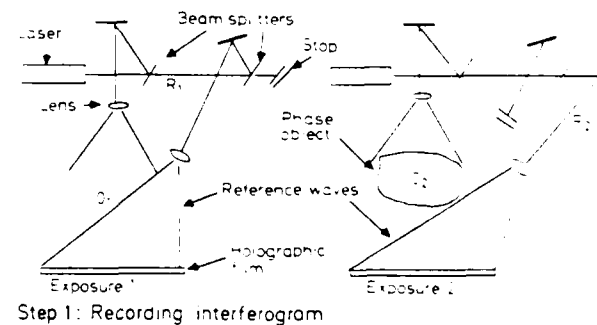


Fig. 1. Schematic setup for digital interferometry of phase objects

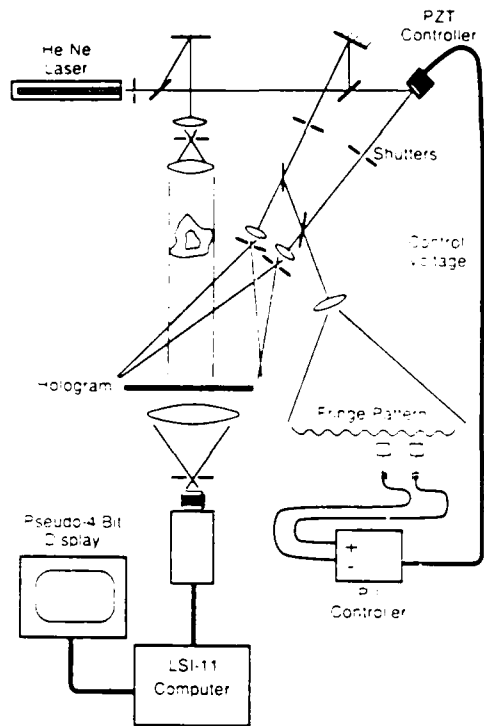


Fig. 2. Experimental setup for plane wave digital interferometry

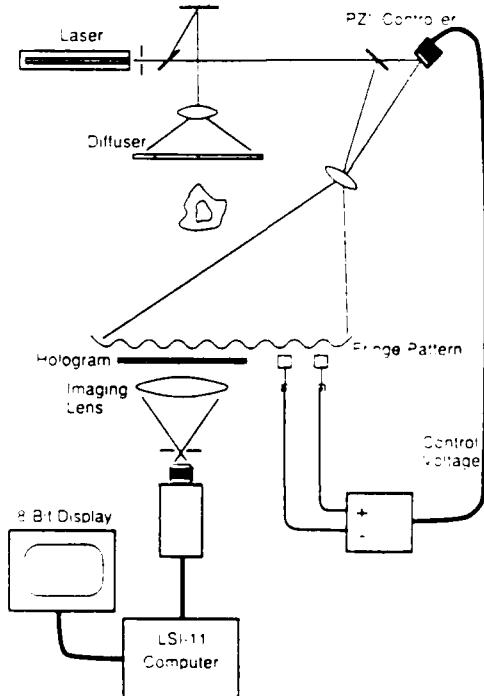


Fig. 3. Experimental setup for diffuse-illumination digital interferometry

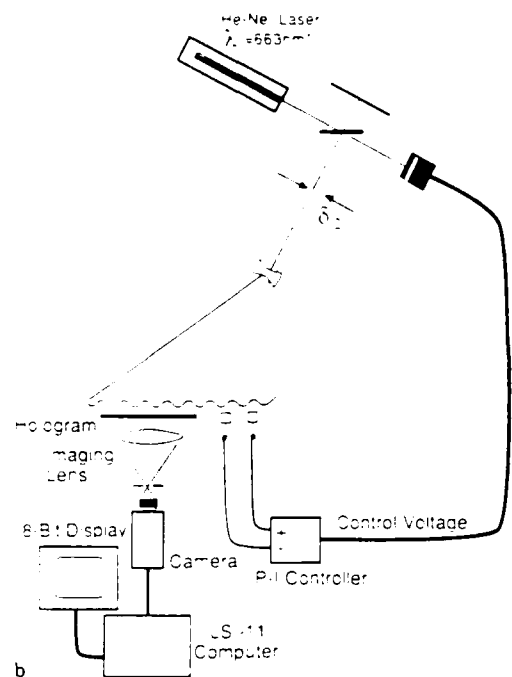
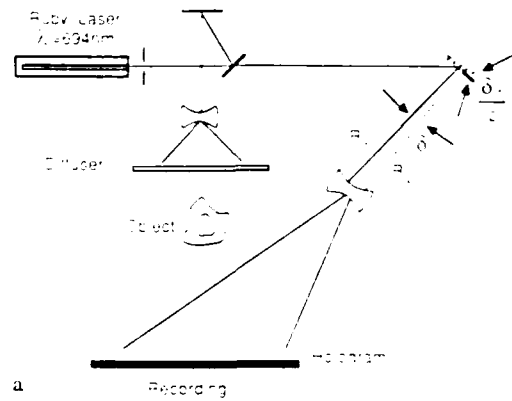


Fig. 4a and b. Setup for a recording and b processing pulsed-laser digital interferogram

images are displaced in the image plane by an amount greater than the speckle size. This overlap reduces the fringe contrast, but does not significantly reduce the accuracy (Dändliker et al. 1982). The small angular separation of the two reference waves causes a regular, visible fringe pattern to be present on the hologram surface, which causes a periodic error. This effect is minimized by placing a low f-number imaging lens very close to the hologram so that the regular fringe pattern is outside the field of focus.

Breuckmann and Thieme (1985) used this arrangement to correct for errors due to wavelength shift when performing digital interferometry when the recording and reconstruction lasers had different wavelengths (see Fig. 4a and b). In this case, the bias phase is given by:

$$\varphi = (k_1 r_1 - k_2 r_1) - (k_1 r_2 - k_2 r_2) + k_2 \Delta r_2$$

where $k_1 = \frac{2\pi}{\lambda_1}$, $k_2 = \frac{2\pi}{\lambda_2}$, $\lambda_1 =$ recording wavelength, $\lambda_2 =$ reconstruction wavelength, or

$$\Delta\varphi = k_1(r_1 - r_2) - k_2(r'_1 - r'_2) + k_2\Delta r'_2.$$

For reference beams separated by a small angle δ whose bisector forms an angle θ with the hologram plane:

$$r_1 - r_2 = r \cos \theta \sin \delta.$$

Thus:

$$\Delta\varphi = 2\pi r \left(\frac{\cos \theta \sin \delta_1}{\lambda_1} - \frac{\cos \theta \sin \delta_2}{\lambda_2} \right) + k_2\Delta r'_2.$$

The terms of the form $\frac{\cos \theta \sin \delta}{\lambda}$ can be shown to be the frequency of the fringe pattern formed by the two reference waves in the hologram plane. Therefore, by setting δ_2 such that the fringe spacing of the reconstruction reference waves is equal to a pattern that would be formed by the two recording reference waves, the chromatic errors in the phase are eliminated. This allows the interferometric phase to be evaluated in the usual way

3 Experimental setup

A digital interferometer with a plane object wave is shown in Fig. 2. The two reference waves are separated by about 20° . The hologram was held and developed in a real-time liquid gate to reduce alignment errors. A second set of experiments was made with diffused illumination (Fig. 4) using a pulsed ruby laser for recording and a He-Ne laser for reconstruction in a manner described by Breuckmann and Thieme (1985). The second recording reference wave was derived in this case by tilting a mirror in the original reference beam by about 0.5° . The hologram is reconstructed with a He-Ne laser using a Michelson interferometer to create the desired fringe pattern. In both cases the phase shifting is done by translating a mirror in one of the reference beams a fraction of a wavelength. The mirror is mounted on a piezoelectric cell, to which a control voltage is applied. In both cases, the two reference waves are brought together to form a fringe pattern which serves as a measure of their mutual phase difference. A pair of photodiodes are placed in the fringe pattern and the error signal between them is used with a proportional-integral

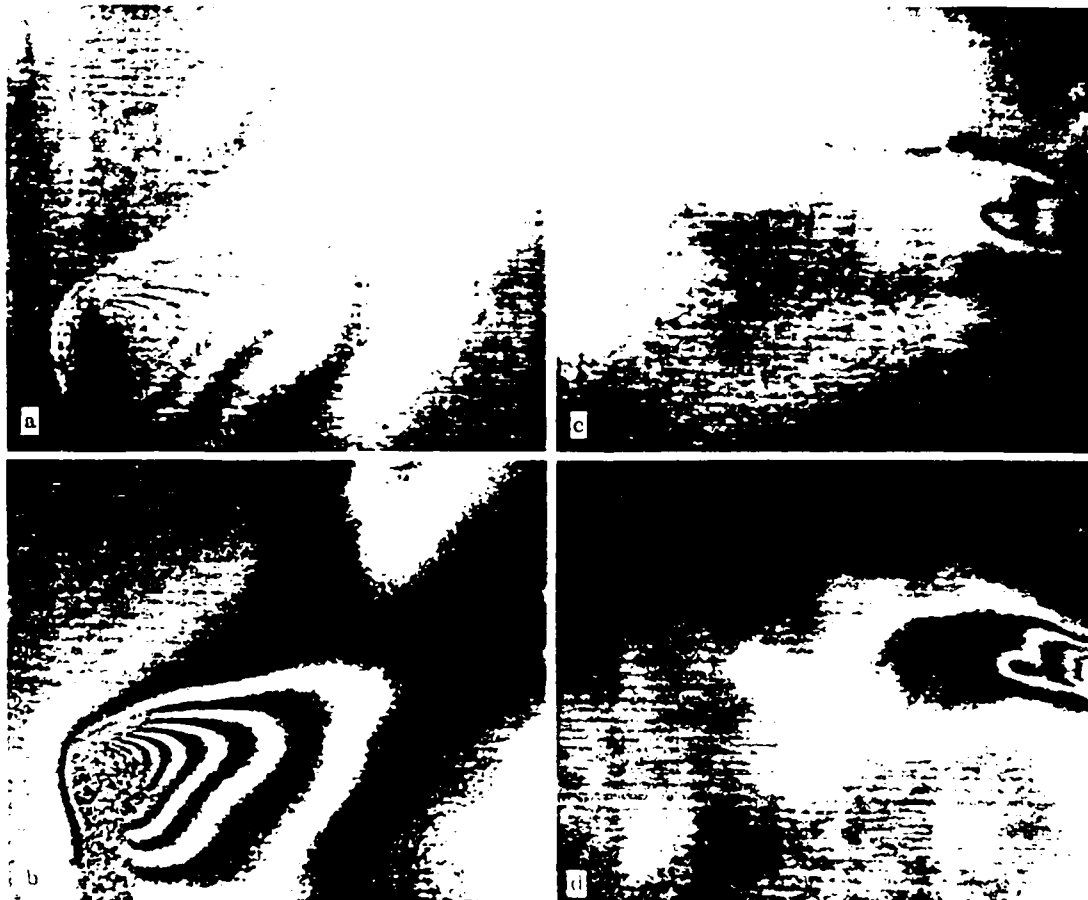


Fig. 5. a Interferogram of strong plume from a heated wire in a cross flow. b phase display of interferogram in a. c interferogram of weakly-heated wire in a cross-flow. d phase display of interferogram in c

controller to generate the control voltage for the piezo-electric cell to maintain a stable fringe pattern (and therefore phase shift) in the presence of electrical, mechanical and thermal perturbations. The plane wave interferographic images were made with a 128 by 128 pixel array CID camera while the diffuse-illumination images were made with a video camera in conjunction with a 256 by 384 pixel video frame store. Each pixel has 255 gray levels. Image computations were done on an LSI-11 based computer, which is interfaced with the camera.

4 Results

The plane-wave interferometer was used to visualize the flow around a cylindrical heated wire. Figure 5a shows the digitized interferogram of a strong, laminar plume while Fig. 5b shows the gray scale display of the phase, modulo 2π . The conversion of the fringe pattern to a linear discontinuous function is evident. Figure 5c shows the digitized interferogram of a slightly heated wire in a cross-flow. This interferogram consists of a few narrowly spaced fringes near the wire and a single broad, indistinct fringe in the wake. The phase display of this interferogram (Fig. 5d) has a greatly enhanced contrast that clearly shows thermal variation in the wake, which is not apparent in the interferogram.

The diffuse-illumination interferometer was used to visualize a nominally axisymmetric, turbulent, helium jet injected in still air. The interferogram shown in Fig. 6a is complicated and difficult to interpret especially near the jet center where the fringes become broad and indistinct. The phase display (Fig. 6b) is an improvement, producing a contour map of the phase. Using a sorting procedure based on the nature of discontinuities in the phase

display, we can compute the total phase at each point in the image. Displaying this total phase as a gray scale (normalized to 255 gray levels) yields the image in Fig. 6c. This image represents a true integral projection of the density of the jet. Close examination of this image reveals two interesting features. The first is the axial distribution of areas of high concentration of helium. The second is the presence of large inclusions of unmixed ambient fluid near the center line of the jet. Although the implications of these structures will not be discussed here, it is interesting to compare the absolute phase plot to the schlieren images of a similar jet made by Crow and Champagne (1971) and the laser-induced fluorescence images of Dimotakis et al. (1983). The schlieren pictures show an apparent fine-grained "surface" of the jet with little indication of the internal structure. The integral phase plot is similar to the centerline laser fluorescence pictures, in that both indicate areas of high jet fluid concentration and large inclusions of unmixed ambient fluid. This is somewhat surprising because the integration would tend to average out the effects of locally strong variation in the concentration field. Further study of such images could be used to examine the symmetry properties of the jets and other mixing phenomena.

5 Applications

These examples point out the potential utility of digital interferometry for flow visualization and measurement. It greatly enhances the image contrast of interferograms of weakly refracting flows, removes the sign ambiguity associated with conventional interferograms, and produces images that display rather subtly flow features. These features could allow unique applications of interferometry.



Fig. 6. a Pulsed laser interferogram of a round, helium jet ($Re = 2,500$). b phase display of a. gray scale display of absolute phase of a.

to flow visualization, such as using small temperature variations as tracers of vorticity in non-buoyant, two-dimensional flows and generation of stereoscopic images of three-dimensional scalar fields. Furthermore, the technique's accuracy, high spatial resolution, and facility of operation indicate potential for making spatially distributed scalar measurements.

Two-dimensional scalar fields may be evaluated directly from the phase, the experimental geometry and the constitutive relation of the refractive index to the scalar quantity of interest (e.g. the Gladstone-Dale relation). Cross-sections of three-dimensional fields may be evaluated using optical tomography, a technique for recovering the cross-sectional distributions of a field from its integral projections (Sweeney & Vest 1973, Vest 1979). A large number of contiguous cross-sections could be obtained from a set of projection images, allowing three dimensional maps of the field to be calculated. This would allow investigation of the structure of the scalar distribution. We have a system for doing this underdevelopment.

The technique also has the potential for determining the concentration in multicomponent mixtures through the use of simultaneous interferograms with several different wavelengths. Since each component has a different specific refractivity at each wavelength, the phase measurement in each wavelength is a linear combination of the concentration of each constituent, implying a unique relation between the phase measurements and the constituent concentrations. The technique's sensitivity and its ability to register efficiently the various interferograms could make such a system practical.

Acknowledgement

This work was sponsored by the Office of Army Research.

References

- Breuckmann, B.; Thieme, W. 1985: Computer-aided analysis of holographic interferograms using the phase shift method. *Appl. Opt.* 24, 2145-2149
- Brown, G. L.; Roshko, A. 1974: On density effects and large structures of turbulent mixing layers. *J. Fluid Mech.* 64, 775-816
- Crow, S. C.; Champagne, F. H. 1971: Orderly structures in jet turbulence. *J. Fluid Mech.* 48, 547-591
- Dändliker, R.; Moram, E.; Mottier, F. M. 1976: Two-reference beam holographic interferometry. *J. Opt. Soc. Am.* 60, 23-30
- Dändliker, R.; Thalmann, R.; Willemin, J.-F. 1982: Fringe interpolation by two reference beam holographic interferometry. *Opt. Commun.* 42, 23-29
- Dändliker, R.; Thalmann, R. 1985: Heterodyne and quasi-heterodyne holographic interferometry. *Opt. Eng.* 24, 824-831
- Dimotakis, P. E.; Miake-Lye, R. C.; Papantoniou, D. A. 1983: Structure and dynamics of round, turbulent jets. *Phys. Fluids* 26, 3185-3192
- Hariharan, P. 1985: Quasi-heterodyne holographic interferometry. *Opt. Eng.* 24, 632-638
- Hariharan, P.; Oreb, P. F.; Brown, N. 1982: A digital phase measurement system for real time holographic interferometry. *Opt. Commun.* 41, 393-396
- Sweeney, D. W.; Vest, C. M. 1973: Reconstruction of three-dimensional refractive index fields from multidirectional interferometric data. *Appl. Opt.* 12, 2649-2664
- Vest, C. M. 1979: *Holographic interferometry*. New York: Wiley

Received November 10, 1986

END

DATE

FILMED

5-88

DTIC